Analysis of CHD-7 defective dauer nematodes implicates collagen misregulation in CHARGE syndrome features.

Diego M. Jofré[1*], Dane K. Hoffman[2*§], Ailen S. Cervino[3], McKenzie Grundy[2], Sijung Yun[4], Francis RG. Amrit[5], Donna B. Stolz[6], Esteban Salvatore[7], Fabiana A. Rossi[8], Arjumand Ghazi[5,9] , M. Cecilia Cirio[3], Judith L. Yanowitz[2,10#], Daniel Hochbaum[1#]

*Authors contributed equally.

[#]Co-corresponding authors.

[1] Departamento de Biodiversidad y Biología Experimental, Facultad de Ciencias Exactas y Naturales, Universidad de Buenos Aires (UBA). Buenos Aires, Argentina.

[2] Magee-Womens Research Institute. Pittsburgh, PA, USA.

[3] Instituto de Fisiología, Biología Molecular y Neurociencias (IFIBYNE-UBA-CONICET), Facultad de Ciencias Exactas y Naturales, Universidad de Buenos Aires (UBA). Buenos Aires, Argentina.

[4] Laboratory of Molecular Biology, National Institute of Diabetes and Digestive and Kidney Diseases, National Institutes of Health. Bethesda, Maryland, USA.

[5] Department of Pediatrics, University of Pittsburgh School of Medicine. Pittsburgh, PA, USA.

[6] Center for Biologic Imaging, University of Pittsburgh Medical School. Pittsburgh, PA, USA.

[7] mAbxience S.A.U. Buenos Aires, Argentina.

[8] Instituto de Investigaciones en Medicina Traslacional (IIMT) - CONICET, Universidad Austral. Pilar, Buenos Aires, Argentina.

[9] Departments of Developmental Biology and Cell Biology & Physiology, University of Pittsburgh School of Medicine. Pittsburgh, PA, USA.

[10] Departments of Obstetrics, Gynecology & Reproductive Sciences; Developmental Biology; Microbiology and Molecular Genetics at he Hillman Cancer Center, University of Pittsburgh. Pittsburgh, PA, USA.

[§]Current Address: Department of Cancer & Cell Biology. Baylor College of Medicine. Houston, Texas, USA.

***Correspondence:** Correspondence should be addressed to

Dr. Daniel Hochbaum
Ciudad Universitaria. Intendente Guiraldes 2160, 4 piso. Laboratorio 79
CABA, Buenos Aires.
C1428BGA
Argentina
hochbaumd@bg.fcen.uba.ar

Dr. Judith L. Yanowitz
Magee-Womens Research Institute
204 Craft Avenue
Pittsburgh, PA
15213
United States of America
yanowitzjl@mwri.magee.edu

Author Contributions

Conceived and designed the experiments: DMJ, DKH, ASC, FAG, ES, MCC, JLY, DH. Performed the experiments: DMJ, DKH, ASC, MG, FRGA, DBS, ES, FAR, DH. Analyzed the data: DMJ, DKH, ASC, SY, FRGA, AG, MCC, JLY, DH. Drafted the manuscript: MCC, JLY, DH. Reviewed and edited the manuscript: DMJ, DKH, AG, MCC, JLY, DH.

Conflict of Interest

The authors declare no conflicts of interest

Classification: Biological Sciences, Developmental Biology.

Keywords: CHARGE Syndrome, *C. elegans*, dauer, TGF-β, Col2a1

This PDF file includes:

Main Text
Figures 1 to 5
Supplementary figures 1-6 and Supplementary Tables S1-S4

ABSTRACT

CHARGE syndrome is a complex developmental disorder caused by mutations in the chromodomain helicase DNA-binding protein7 (CHD7) and characterized by retarded growth and malformations in the heart and nervous system. Despite the public health relevance of this disorder, relevant targets of CHD7 that relate to disease pathology are still poorly understood. Here we report that *chd-7*, the nematode ortholog of Chd7, is required for dauer morphogenesis, lifespan determination, and stress response. Consistent with our discoveries, we found *chd-7* to be allelic to *scd-3*, a previously identified dauer suppressor from the TGF-β pathway. Notably, DAF-12 promoted *chd*-7 expression, which is necessary to repress *daf-9* for execution of the dauer program. Transcriptomic analysis comparing *chd-7*–defective and normal dauers showed enrichment of collagen genes, consistent with a conserved role for the TGF-β pathway in formation of the extracellular matrix. To validate a conserved function for *chd-7* in vertebrates, we used *Xenopus laevis* embryos, an established model to study craniofacial development. Morpholino mediated knockdown of Chd7 led to a reduction in *col2a1* mRNA levels. Both embryonic lethality and craniofacial defects in Chd7-depleted tadpoles were partially rescued by over-expression of *col2a1* mRNA. We suggest that pathogenic features of CHARGE syndrome caused by Chd7 mutations, such as craniofacial malformations, result from the reduction of collagen levels, implying that the extracellular matrix might represent a critical target of Chd7 in CHARGE development.

SIGNIFICANCE STATEMENT

CHARGE Syndrome is a complex developmental disorder caused by mutations in the chromodomain helicase DNA-binding protein-7 (CHD7). Unfortunately, the cellular events that lead to CHARGE syndrome are still poorly understood. In *C. elegans*, we identified *chd-7* in a screen for suppressors of dauer formation, an alternative larval stage that develops in response to sensory signals of a harsh environment. We found that *chd-7* regulates expression of collagens, which constitute the worm's cuticle, a specialized extracellular matrix. In frog's embryos, we show that Chd7 inhibition leads to poor Col2a1, which is necessary and sufficient to exhibit CHARGE features. These studies establish *C. elegans* as an amenable animal model to study the etiology of the developmental defects associated with pathogenic Chd7.

INTRODUCTION

CHARGE syndrome is a rare and severe neurodevelopmental disorder that affects the neural tube and neural crest cell derivatives, leading to hypogonadism, heart defects and craniofacial anomalies among other features (1). Inactivating mutations in *CHD7* (chromodomain-helicase-DNA binding 7) are the predominant cause of CHARGE, accounting for greater than 90% of the cases (2). *CHD7* is also mutated in Kallmann syndrome, a milder neurodevelopmental disorder with features overlapping with CHARGE, including impaired olfaction and hypogonadism (3). Exome sequencing studies in patients with autism spectrum disorders (ASDs) identified recurrent disruptive mutations in the related gene *CHD8* (4). The CHD proteins comprise a highly conserved family of SNF2-related ATP-dependent chromatin remodelers that are involved in chromatin remodeling and transcriptional regulation (5). Despite the public health relevance of these cognitive disorders, the mechanism of disease pathology due to mutations in CHD7/8 is poorly understood. The development of fly, fish and mouse models of CHARGE has abetted in characterization of associated dysfunction, but our understanding of the underlying pathology of CHARGE is still incomplete (6–11). CHD-7 is the ortholog of human CHD7 and CHD8 in *Caenorhabditis elegans* and has functions in habituation learning, normal locomotion, body size and fecundity (12, 13). It contains a conserved ATPase/SNF2 domain and two chromodomains for nucleosome interaction. Being the only worm homolog of the Class III CHD family, it contains a signature BRK domain (Brahma and Kismet domain) (Figure 1E).

When *C. elegans* encounter crowding, starvation or high temperature during early development, worms can halt reproductive programs to enter an alternative larval stage known as dauer. Dauers are long-lived, highly stress resistant and exhibit altered motility and metabolism (14–17). Upon return to normal growth conditions, the larvae exit dauer and develop into fertile adults. Study of dauer formation mutants has provided fundamental insights into pathways affecting longevity, neurodevelopment, metabolism, autophagy and neurodegeneration (14, 17–20).

The DAF-2/insulin/IGF- signaling 1 (IIS) pathway controls the dauer entry decision by coupling external cues with neuroendocrine signaling (21). In favorable conditions, DAF-2 activity initiates a conserved kinase cascade, leading to phosphorylation and inhibition of the transcription factor DAF-16/FOXO. In harsh environments, a decrease in the activity of DAF-2 and downstream components of the pathway leads to activation of DAF-16 and causes animals to arrest as dauers (22, 23). In addition to the DAF-2 pathway, DAF-7/ TGF-β signaling also regulates dauer development (24). When worms sense suitable conditions for reproductive development, ASI neurosensory cells secrete DAF-7, which binds to DAF-1/4 receptors leading to activation and phosphorylation of the R-SMAD complex DAF-8/14, promoting reproductive programs and inhibiting the pro-dauer complex composed of the SMAD protein DAF-3 and repressor DAF-5. Conversely, absence of DAF-7 leads to activation of the DAF-3/DAF-5 complex to promote dauer entry (25, 26).

139 DAF-7/TGF-β and DAF-2/IIS pathway were initially described as parallel pathways to regulate dauer entry
140 (27), but recent observations suggest a strong positive feedback between these pathways for dauer entry
141 and longevity (15–20). First, decreased signaling through the TGF-β pathway leads to differential
142 expression of many DAF-16 regulated genes with functions in longevity and dauer entry, such as SOD-3
143 or insulin peptides. This cross-activation of target genes may be important to amplify weak signals from
144 each sensory pathway to make an all-or-none decision to enter dauer (28–30). Second, the longevity of
145 *daf-2* mutants can be blocked or enhanced by *daf-5* and *daf-3*, respectively, suggesting that
146 transcriptional components of the TGF-β can modulate IIS-dependent longevity genes. Third, for dauer
147 development, *daf-16* is epistatic to *daf-7/8/14 daf-c* mutants (30, 31). Lastly, both signaling pathways
148 converge on *daf-9* and *daf-12* to integrate outputs for diapause entry (32, 33). Indeed, *daf-9* expression
149 levels is critical for both entering and exiting diapause (17, 32).
150 In chromatin immunoprecipitation (ChIP)-chip studies, we identified *chd*-7 as a DAF-12 target
151 gene whose loss caused defective execution of dauer morphogenesis programs (34). We show that while
152 CHD-7 can modulate multiple IIS-associated processes, including *daf-2(e1370)* dauer formation,
153 longevity and immunity, epistatic experiments place *chd-7* in the DAF-7/TGF-β pathway. Whole genome
154 mRNA expression profiling of partial dauers show that *chd-7* mutants fail to repress *daf-9* during dauer
155 development, preventing developmental arrest of the constitutive dauer mutant *daf-7(e1372)*. In addition,
156 we found collagens to be among the most differentially regulated genes, consistent with a known role for
157 the TGF-β pathway in regulating components of the extracellular matrix (35).To validate a conserved
158 function for *chd-7* in vertebrates and study the relevance of our results for CHARGE etiology, we used
159 *Xenopus laevis*. Disruption of Chd7 function in *Xenopus* embryos results in craniofacial defects that mimic
160 CHD-dependent pathological phenotypes (36, 37). We demonstrate that Chd7 regulates expression of
161 the collagen type-II, alpha 1, *col2a1*, the main collagen protein of cartilage (38). Interestingly, craniofacial
162 malformations and embryonic lethality due to *chd7* knockdown can be rescued by *col2a1* expression.
163 These findings suggest a conserved function of *chd7*/*chd-7* in regulation of extracellular matrix
164 components and raise the intriguing possibility that defects in collagen expression may contribute to the
165 craniofacial defects seen in CHD7/8-dependent syndromes.
166
167 **RESULTS**
168
169 ***chd-7* functions in development of the dauer larva**
170 Previously, we identified ~3000 potential DAF-12 target genes by ChIP-chip (34). We reasoned
171 that among these genes would be novel regulators of dauer development. To identify such genes, we
172 took advantage of the temperature-sensitive, constitutive dauer (Daf-c) allele *daf-2(e1371)*. At the non-
173 permissive temperature of 25°C, all the offspring enter the dauer phase and become SDS resistant (22).
174 We expected that inactivating targets of DAF-12 that function in dauer formation should suppress the Daf-

175 c phenotype of *daf-2* and produce either defective, SDS-sensitive "partial" dauers or reproductive adults.
176 To confirm these results, we assayed suppression of the more severe *daf-2(e1370)* mutation and
177 discovered that *chd-7(RNAi)* produced arrested, SDS-sensitive larvae, indicative of the partial dauer
178 phenotype (39). As observed in Figure 1A and B, the axial ratio (length/width) of the partial dauers
179 resulting from *chd-7(RNAi)* exhibited a significant reduction of these proportions and appeared to have
180 defects in radial constriction of the dauer cuticle. By using a *chd-7* transcriptional reporter
181 (WBStrain00033709), we observed a substantial decrease in *chd-7* expression in the *daf-12(rh61rh411)*
182 background (Figure 1C and D). Thus, we infer that DAF-12 binds to the *chd-7* promoter (34) and
183 upregulates its expression.
184 To further validate our screen, we crossed *daf-2(e1370)* mutants with three *chd-7* deletion alleles
185 available from the Nematode Knockout Consortia (40). Allele *chd-7(tm6139)* contains a 594bp deletion
186 that generates a frame shift and premature stop codon, eliminating all known protein domains (Figure
187 1E). As shown in Figure 1F, SDS-sensitive dauers were obtained when double mutants are grown at
188 25°C, validating our screen. Comparison of two partial deletion alleles uncovered a critical role for the
189 BRK domain in dauer formation. The *chd-7(gk290)* allele contains a 859bp deletion that spans the BRK
190 domain and introduces a frameshift that eliminates the last 356aa. The *chd-7(gk306)* deletion is slightly
191 more C-terminal, truncating the protein immediately after the BRK domain (Figure 1E). When crossed into
192 *daf-2(e1370)* worms, *chd-7(gk306)* developed normal, SDS-resistant dauer larvae, whereas *chd-7(gk290)*
193 formed partial dauers that were sensitive to detergent (Figure 1F). Importantly, a functional transgene
194 expressing GFP-tagged CHD-7 protein (CHD-7::GFP) rescued the partial dauer phenotypes observed in
195 *chd-7(gk290);daf-2(e1370)* and *chd-7(tm6139);daf-2(e1370)* mutants (Figure 1F).
196 The dauer larva is characterized by a slim physique because of a reduction in the volume of
197 ectodermal tissues, including the hypodermis, seam cells and pharyngeal cells. In addition, the
198 hypodermis produces the dauer cuticle, which confers protection against external damage and
199 dehydration. During development, the seam cells fuse and the multinucleate cells produce the alae-
200 bilateral ridges in the cuticle that facilitate body motion. Dauer larvae also switch their metabolism to
201 accumulate lipids to survive for longer periods. To further characterize the nature of the defects in the
202 *chd-7*-induced partial dauers, we first studied the seam cells fusions with the adherens junction-
203 associated protein marker AJM-1::GFP and the morphology of the cuticle with scanning electron
204 microscopy (SEM). In dauering preparation, animals store fat in their intestinal and hypodermal cells,
205 which is critical to survive during hibernation (41). As shown in Figure 1G, partial dauers exhibited defects
206 in seam cell fusion and defective dauer alae formation. Next we used the lipid-labeling dye, Oil Red O
207 (ORO), to examine fat storage and found that, unlike other partial dauer mutants (19), the *chd-7;daf-2*
208 abnormal dauers did not exhibit fat-storage deficiencies (Supplemental Figure 1).
209 During dauer, the global developmental arrest also impacts the germ cells, slowing their divisions
210 and finally remaining quiescent (42). We observed that the germ line in *chd-7* mutant dauers was

211 substantially larger than in control dauers and appeared to arrest with a germline morphology resembling
212 that seen in L3 larval stage (Figure 1H). Therefore, we conclude that major morphological changes that
213 occur during dauer formation fail to be executed in *chd-7* mutants, including radial constriction of the
214 body, formation of an SDS-resistant cuticle with dauer alae, and developmental arrest of the germ line.
215
216 ***chd-7* is required for longevity and immunoresistance induced by IIS inactivation and germline**
217 **removal**
218 In addition to dauer development, the IIS pathway also regulates longevity (14). Hence, we
219 sought to investigate whether *chd-7* also has roles in the determination of lifespan. First, we compared
220 survival of wild-type (N2) worms with two *chd-7* alleles and found that the dauer-defective allele *chd-*
221 *7(gk290)* significantly shortened lifespan, whereas *chd-7(gk306)* had only a marginal effect on longevity
222 (Figure 2A). Surprisingly, the CHD-7::GFP rescue transgene also reduced N2 lifespan (Figure 2B),
223 suggesting that *chd-7* copy number can influence longevity. We then analyzed how *chd-7* affects
224 longevity of IIS mutants. Remarkably, the dauer suppressor allele *chd-7(gk290),* but not *chd-7(gk306),*
225 shortened the lifespan extension of *daf-2* mutants to an extent comparable with the null allele of *daf-16,*
226 the key IIS downstream target (Figure 2C) (14). Furthermore, *daf-2* longevity was fully restored by CHD-
227 7::GFP (Figure 2D).
228 To determine if the effects on lifespan were specific to the IIS pathway, we assayed the
229 contribution of *chd-7* to the longevity induced by germ cell-less mutations, a longevity paradigm that
230 operates in parallel to IIS. Temperature-sensitive *glp-1(e2144)* animals are sterile and long-lived at non-
231 permissive temperatures (43). This lifespan extension was dependent on *chd-7*, as *chd-7(gk290);glp-*
232 *1(e2144)* double mutants had a mean lifespan significantly shorter than *glp-1(e2144)* single mutants
233 (Figure 2E). The impact was similar to that produced by absence of the nuclear receptor *daf-12* (Figure
234 2C), which is strictly necessary for germless longevity (43).
235 In addition to longevity, IIS reduction also enhances resistance against multiple stressors
236 including pathogen attack and starvation. We asked if *chd-7* inactivation impaired *daf-2*
237 immunoresistance too. As shown in Figure 2F, *chd-7* mutants repressed the increased survival of *daf-2*
238 worms upon exposure to the human opportunistic pathogen, *Pseudomonas aeruginosa* strain PA14 (44).
239 In contrast, *chd-7* had a modest effect on survival of wild-type worms' pathogen resistance. Furthermore,
240 the *chd-7(gk290)* and *chd-7(tm6139)* alleles reduced the survival of *daf-2(e1370)* L1 larvae subjected to
241 starvation stress (Supplemental Figure 2) (45). Taken together, these results suggest that *chd-7* mediates
242 the increased lifespan of at least two longevity paradigms (IIS mutants and germ cell-less animals), as
243 well as the response to pathogens and starvation.
244
245
246

247 **CHD-7 is a member of the TGF-β pathway**

248 Since our genetic analyses implicated *chd-7* as a dauer defective mutant (Daf-d) in the IIS
249 signaling pathway (Figure 1), we sought to understand whether it also had roles in the TGF-β dauer
250 pathway (27, 28). As shown in Figure 3A, at the restrictive temperature of 25°C, *chd-7*;*daf-7(e1372)*
251 double mutants bypassed the dauer arrest to become fertile adults. For *daf-5*, which acts as a dauer
252 suppressor of the TGF-β pathway, the Daf-d phenotype is observed at 25°C, but at a slightly higher
253 temperature, suppression is incomplete (26). Thus, we asked whether *chd-7* also prevented dauer arrest
254 at higher temperatures. As shown in Figure 3A, *daf-7*-dependent arrest was recapitulated at 26.5°C,
255 suggesting that *chd-7* has a Hid (high temperature-induced dauer formation) phenotype (46). As expected
256 for a putative transcriptional regulator, epistasis analysis placed CHD-7 downstream of the receptor DAF-
257 1 and the R-Smad DAF-14 (Figure 3B).

258 In addition to dauer formation, the TGF-β signaling pathway also regulates body size and male
259 tale development, mainly through the ligand DBL-1 (47, 48). To test if *chd-7* impacted these processes as
260 well, we measured the length of *chd-7* young adults and found them to be significantly shorter than N2
261 control animals (Figure 3C). We also observed that males carrying the severe loss-of-function allele *chd-*
262 *7(tm6139)* failed to mate with *fog-2* mutant females (Figure 3D) due to defects in male tail development
263 (not shown). This male infertility was rescued by the CHD-7::GFP transgene (Figure 3D).

264 More than twenty years ago, in a screen for suppressors of dauer formation within the TGF-β
265 pathway, *Inoue et al.* identified three complementation groups (31). We noticed that one of these, *scd-3*
266 (suppressor of constitutive dauer-3), was located between *unc-11* and *dpy-5* on chromosome I, in the
267 same genetic region as *chd-7*. Features of *scd-3(sa253)* worms include low brood size, egg-laying
268 defects (Egl), short body size (Dpy) and male abnormal defects (Mab), all of which were phenotypes
269 shared with *chd-7* as described above. In addition, improper gonad migration is a common phenotype of
270 *scd-3* and *chd-7* mutants (Supplemental Figure 4). To determine if *chd-7* and *scd-3* are allelic, we
271 sequenced *scd-3(sa253)* and found a single G/A mutation in exon 8 of the *chd-7* locus, that introduces a
272 premature STOP codon at position Q2422, eliminating the BRK domain of CHD-7 protein, confirming that
273 *chd-7* is *scd-3* (Figure 1E).

274

275 **Transcriptomics analysis identifies *daf-9* and collagens as targets of CHD-7**

276 To gain further insight into the role of CHD-7 in dauer development, we performed RNA-Seq. We
277 compared the transcriptomes of *daf-2(e1370)* dauers and *chd-7(gk290);daf-2(e1370)* partial dauers.
278 Differentially expressed genes (DEGs) analysis revealed that decreased expression of 28 genes and
279 increased expression of 56 genes in the double mutants (Figure 4A and Supplemental Table 3). Among
280 the latter group, we found *daf-9,* encoding the cytochrome p450 that integrates inputs from TGF-β and
281 insulin/IGF-II pathways to regulate DAF-12 activity during dauer development (49). We confirmed the
282 increased expression of *daf-9* upon *chd-7* loss by RT-qPCR (Figure 4B). We hypothesized that *daf-9*

283 expression levels must be critical in the decision to develop as either fertile adults or to enter diapause,
284 and therefore the increased expression of *daf-9* in the *chd-7;daf-2* double mutants may be preventing full
285 execution of the dauer program. Consistent with this hypothesis, we found that depletion of *daf-9* in
286 *chd7*;*daf-7* animals restored the dauer arrest phenotype at the non-permissive temperature of 25°C
287 (Figure 4C). However, these animals still appeared to be detergent-sensitive partial dauers (Figure 4D),
288 since *daf-9* itself is required for proper dauer morphogenesis (39). Thus, we posit that the inability of *chd-*
289 *7* mutants to fully repress *daf-9* may be sufficient to activate DAF-12 and inhibit dauer formation in both
290 the TGF-β and IIS pathways (Figure 4E).
291 The partial dauer larvae that arise from knockdown of *chd*-7 are short and thick and lack dauer
292 alae, indicative of cuticle defects (Figures 1A and 1G). Thus, we reasoned that *chd-7* might also regulate
293 target genes that are required for dauer morphogenesis. Further analysis of our transcriptomic data
294 showed that 10% of the DEGs were collagens (*col-103*, *col-50*, *dpy-2*, *col-184*, *col-141*, *col-142*, *col-42*
295 and *dpy-9*), which are structural components of the cuticle. All these collagens showed increased
296 expression in the *chd-7*-mutant dauer larvae (Figure 4A). FPKM data from Modencode libraries indicates
297 that each of these collagens show very low expression during dauer and are expressed during various
298 stages of reproductive development, suggesting that repression of the genes must be important for dauer
299 development (50). Thus, our results suggest that CHD-7 is required for repression of dauer-specific
300 collagens. These results are consistent with growing evidence that the TGF-β pathway is a major
301 regulator of collagen deposition (35, 51). In fact, it was recently reported that two of our target genes, *col-*
302 *141* and *col-142*, contain SMAD-binding elements (SBEs) and their expression is directly regulated by the
303 TGF-β pathway to determine body size (52).
304 In addition to the transcriptomic analysis of dauers, we analyzed CHD-7's CHIP-seq data
305 generated by the ModEncode project in young adults (Supplemental Table 4). Because the expression
306 profiles of adult TGF-β and IIS mutants show significant overlap and co-regulation of many DAF-16 target
307 genes (28), we compared this analysis with DAF-16 CHIP-seq data also from ModEncode in L4 larvae.
308 To our surprise, we found that both transcriptional regulators share a significant number of genes
309 (Supplemental Figure 5). Along with our observation that *chd-7* is necessary for lifespan extension of *daf-*
310 *2* mutants, these data indicate that *chd-7* could modulate longevity by regulation of the IIS pathway,
311 possibly through direct regulation of target genes.
312
313 **Chd7 regulates *col2a1* during *Xenopus* embryogenesis**
314 Type-II collagen is an extracellular matrix (ECM) protein conserved in all multicellular animals,
315 which forms fibrils (53) and has fundamental roles in development and tissues homeostasis (54). In
316 vertebrates, the fibrillar type-II collagen is the major structural protein of cartilage and plays a prominent
317 role in cranial development in multiple organisms (38, 55). Collagen, type-II, alpha 1 (Col2a1) is the major
318 component of the cartilage matrix having a structural function and being an important extracellular

319 signaling molecule for regulation of chondrocyte proliferation, metabolism, and differentiation (56–58).
320 The African frog *Xenopus laevis* is a well-established model to study vertebrate facial disorders which
321 often arise from defects in neural crest development and migration (37). In *Xenopus* embryos, prior
322 studies established that Chd7 regulates neural crest specification and migration and its depletion
323 recapitulates the craniofacial defects seen in CHARGE patients (36). To investigate whether Chd7 has a
324 conserved mechanism of action and regulates collagen expression in vertebrates, we used a previously
325 validated morpholino to induce *Xenopus* Chd7 knockdown (*chd7*-MO) (36). In *Xenopus,* Col2a1 is
326 essential for normal development of the skeleton and its expression is restricted to the cartilaginous
327 skeleton of the tadpole and adult frog (59). In *chd7*-MO injected embryos, RT-qPCR revealed a significant
328 reduction of *col2a1* mRNAs as compared to control-injected animals (Figure 5A).
329 For targeted disruption of Chd7 function, we injected the dorsal-animal (D1) blastomeres of 8-cell
330 stage embryos fated to contribute to the dorsal anterior structures. *In situ* hybridization of unilaterally
331 injected embryos showed alterations in *col2a1* expression in the branchial arches and/or the otic vesicle
332 (ear vesicle) (59) upon *Chd7* depletion relative to embryos injected with a control morpholino (St-MO)
333 (Figure 5B). The injection of *chd7*-MO into both D1 blastomeres of 8-cell stage embryos with doses
334 between 1.25 ng and 2.5 ng showed 10-20% embryonic mortality (Figure 5C and data not shown). The
335 higher doses of 5 ng and 10 ng led to >50% lethality (Figure 5C). We next sought to investigate if the
336 mortality was related to collagen deficits and therefore conducted rescue experiments by co-expressing
337 *Xenopus col2a1* mRNA with the morpholino. As shown in Figure 5C, coinjection of *col2a1* mRNA
338 substantially improved (~50%) embryo survival relative to the injection of *chd7*-MO alone. We then asked
339 if ectopic *col2a1* mRNAs could suppress the craniofacial defects associated with *chd7* loss-of-function.
340 Initially, we analyzed the gross morphology of the surviving stage 45 tadpoles and observed a high
341 incidence of craniofacial malformations (83%) in Chd7-depleted animals (Supplemental Figure 6A and
342 6C) and a significant reduction upon *col2a1* mRNA coinjection (43%) (Supplemental Figure 6B). Next, we
343 examined eye size and eye distance, since microthalmia and midline defects are often associated with
344 CHARGE syndrome (60) and are recapitulated in *Xenopus* embryos (36). Both eye size and distance
345 between eyes were reduced in Chd7-depleted tadpoles and were partially rescued by *col2a1* mRNA
346 expression (Figure 5D and 5E). Therefore, expression of *col2a1* ameliorated the phenotypes associated
347 with pathogenic Chd7 suggesting that collagen is a conserved and important target of this protein.
348
349 **DISCUSSION**
350
351 We initially identified *chd*-7 in chromatin immunoprecipitation (ChIP)-chip studies of the nuclear
352 receptor DAF-12 (34), a transcription factor regulating worm aging, development, and dauer formation
353 (61), and found it to be critical for *daf-2* mediated dauer development. Comparison of the *chd-7* alleles
354 *gk290* and *gk306* showed a critical role for the BRK domain in dauer development and longevity (Figures

355 1F-H, 2A and 2C). In CHARGE patients, deletions or mutations within the BRK domains of CHD7 are
356 sufficient to elicit all the features characteristic of the disease, underscoring the importance of this domain
357 (62). The phenotypic differences between the worm alleles highlight the potential of the worm to delimit
358 functional domains of CHD-7 that contribute to disease pathology. In mice, homozygous mutations in
359 *Chd7* lead to embryonic lethality at E10.5, in part because *Chd7* is necessary for early brain development
360 (36). In worms, the presumptive null allele c*hd-7(tm6139)* and *scd-3(sa253)* were viable but showed
361 reproductive defects, such as improper gonad proliferation and migration, reduced fecundity, male tail
362 defects and hermaphrodite vulval defects (31), indicating that *C. elegans* are more able to tolerate loss of
363 CHD-7 than mice or humans. Thus, our studies establish *C. elegans* as an animal model to study the
364 mechanisms underlying the developmental defects observed in pathogenic Chd7.
365 Both a *chd-7* mutation and *chd-7* overexpression shortened the lifespan of otherwise wild-type
366 worms, suggesting that CHD-7 proteins levels must be tightly regulated to ensure proper development. Of
367 note, Chd7 is the most commonly amplified gene in tumors amongst the CHD superfamiliy members, and
368 its overexpression is associated with aggressive subtypes of breast cancer and poor prognosis (63).
369 Thus, in humans, as well as worms, gain-of-function phenotypes are associated with Chd7/*chd-7*
370 overexpression.
371 Our genetic epistasis analyses placed CHD-7 downstream of the TGF-β-like DAF-7, the type I
372 receptor DAF-1, and the R-SMAD DAF-14 placing CHD-7 at the level of the Co-Smad DAF-3 and the
373 Sno/Ski repressor DAF-5, which are also Daf-d (64). While *daf-3* and *daf-5* completely suppress dauer
374 formation in a *daf-7* background at 25°C, *daf-5* fails to suppress dauer formation in TGF-β mutants at
375 27°C (26), supporting a role for CHD-7 at the DAF-3/DAF-5 step in the pathway (Figures 3A and 3B).
376 Interestingly, these transcriptional regulators have opposite effects on *daf-2*-induced longevity: *daf-3*
377 enhances *daf-2(e1370)* longevity while *daf-5* mutations suppresses it (30). We observed that *chd-7*
378 suppresses *daf-2* longevity (Figure 2C), like *daf-5(e1386)*. Together these data suggest that CHD-7 either
379 regulates *daf-5* expression or directly interacts with DAF-5 to regulate downstream target genes, or both.
380 In mice, CHD7 was shown to physically interact with SMAD1 and form a transcriptional complex with
381 SMAD4, the mammalian ortholog of DAF-3 (65). We therefore speculate that DAF-3, DAF-5, and CHD-7
382 may be in ternary complex that regulates *daf-9* expression for dauer entry (Figure 4C). Interactome
383 mapping of the TGF-β pathway also identified SWSN-1, a SWI/SNF subunit component of the BAF
384 complex, as a physical interactor of DAF-3 (66). CHD7 interacts with human and *Xenopus* PBAF
385 (polybromo- and BRG1-associated factor-containing complex) to control neural crest gene expression
386 (36). In worms, both *swsn-1* and *chd-7* fail to develop normal dauers in *daf-2* and *daf-7* mutants
387 (Supplemental Figure 3 and (67)). Thus, we envision that CHD-7 may work together with the BAF
388 complex and DAF-3/DAF-5 to control gene expression of target genes critical for dauer formation.
389 DAF-9 activity is necessary and sufficient for the decision to enter diapause: reduced activity of
390 TGF-β and IIS pathways leads to *daf-9* repression and dauer development. Conversely, *daf-9* expression

391 in the hypodermis is sufficient to inhibit diapause, driving reproductive programs in *daf-7* mutants (29, 32).
392 Ectopic *daf-9* expression also drives reproductive programs in the weak *daf-2(e1368)* allele, but only
393 partially suppresses *daf-2(e1370)* diapause leading to arrest as L3 or early L4 larvae (32). Based on
394 these observations, we speculate that *daf-9* misexpression explains a subset of the *chd-7* phenotypes
395 observed herein, including the partial dauer phenotype, gonad migration defects, and vulval protrusions,
396 all of which overlap with published *daf-9* phenotypes (32, 33, 68). Interestingly, *daf-9* is both upstream
397 and downstream of *daf-12* for dauer formation *(32, 33)*. Our data demonstrated that DAF-12 regulates
398 *chd-7* expression and CHD-7 in turn regulates *daf-9* expression. Therefore, we propose that CHD-7
399 belongs to the transcriptional complex that regulates the feedback loop between *daf-12* and *daf-9*.
400 Among the differentially expressed genes, we noted the presence of several G protein coupled
401 receptors (GPCRs), which could be candidate chemoreceptors for dauer pheromone or environmental
402 cues and thus may be required for either dauer entry or maintenance (42). Consistent with our
403 transcriptomic studies, *Liu et al.* analyzed the expression differences between L2/L3 larvae and TGF-β
404 mutants undergoing diapause and found enrichment of collagen genes, GPCRs and *daf-9*, further
405 validating our placement of *CHD-7* in the TGF-β dauer signaling pathway (29). In a more recent paper,
406 also was established that GPCR gene expression increases significantly during dauer commitment (69).
407 In *C. elegans*, the TGF-β family pathway has diversified and has unique ligands and effectors for
408 the control of dauer induction and aspects of somatic development. Mutations in the TGF-β ligand *dbl-1*
409 and its downstream components cause a small body size (Sma phenotype) (47, 48). Consistent with *chd-*
410 *7* being a component of the TGF-β signaling pathway, *chd-7(gk290)* and *chd-7(tm6139)* are significantly
411 shorter than wild-type worms (Figure 3C). This phenotype is also observed in *scd-3* mutants (31). The
412 *dbl-1* pathway mutants have defects in male tale development (48), a phenotype shared in *scd-3* (31) and
413 *chd-7* mutant animals (data not shown and (31)). Therefore, our results suggest that CHD-7 acts as a
414 regulator of both the *daf-7* and *dbl-1* branches of the TGF-β pathway.
415 Craniofacial anomalies seen in CHARGE patients involve tissues deriving from cells of the neural
416 crest, including craniofacial cartilage and bone, heart, ears and eyes (60, 70). *Xenopus laevis* is an
417 established model to understand fundamental questions of craniofacial biology (37). *Chd7* knockdown in
418 frogs and in zebrafish (11, 36), leads to defects in neural crest specification and migration, which was
419 recently been recapitulated in human embryonic stem cells (hESCs) (71). Our RNA-seq analysis revealed
420 that CHD-7 regulates expression of genes from the cuticle, a modified extracellular matrix (72). Here, we
421 show a role for Chd7 in regulating *col2a1* expression, a type II collagen and the major component of
422 cartilage (55). Interestingly, regulation of *col2a1* by Chd7 is also observed in zebrafish (73). While
423 additional studies are required, we speculate that Chd7 could regulate *col2a1* in a complex with the
424 transcription factor Sox10 (74, 75) or through the TGF-β signaling pathway (35, 76). Supporting the latter
425 mechanism, it was demonstrated in chondrocytes that TGF-β regulates *col2a1* expression (77, 78). Taken

426 together, our data supports a model in which collagen misexpression by pathogenic Chd7 leads to
427 craniofacial defects and embryonic lethality.
428
429 **MATERIALS and METHODS**
430
431 ***C. elegans* strains**
432 All strains were grown and maintained on standard nematode growth medium (NGM). In
433 Argentina (Hochbaum lab), plates were supplemented with 0.1 mg/ml streptomycin and 100 U/ml Nystatin
434 using the *E. coli* OP50-1 strain as the food source. In Pittsburgh (Yanowitz lab), strains were grown on
435 standard NGM seeded with OP50. Temperature-sensitive strains were maintained at 16°C and shifted to
436 the non-permissive temperature of 25°C to induce dauer formation, unless otherwise indicated. All other
437 strains were maintained at 20°C. All *daf-7* strains were maintained at low density to prevent dauer
438 induction at 16°C. Dauer studies were performed in both the Yanowitz and Hochbaum laboratories to
439 validate results. All *chd-7* alleles were outcrossed at least 5 times prior to use.
440 Strains utilized in this study are listed in Supplemental Table 1. Standard genetic crosses were
441 used to make double or triple mutants. The presence of mutant alleles was confirmed a) by the *daf-c*
442 phenotypes in animals heterozygous for additional mutations and b) by PCR and/or sequencing for all
443 additional mutations.
444
445 **RNAi screen for dauer suppressors**
446 All RNAi clones were picked from the Ahringer bacterial feeding library (79). These *E. coli* clones
447 were seeded on NGM plates supplemented with 1 mM of IPTG (Isopropyl β-D-1-thiogalactopyranoside)
448 and 0.1 µg/ml ampicillin, and used for inducing RNAi by the feeding method (80).
449 GL228 [*rrf-3(pk1426)*] II;*daf-2(e1371)* III] eggs were placed in 24-well RNAi plates seeded with
450 bacteria expressing the dsRNA of interest. Worms were maintained for 5 days at 15ºC until adulthood,
451 then were transferred to an identical 24-well plate to lay eggs for 5 h. Adults were removed and the eggs
452 were incubated at 25°C for 4 days to allow formation of dauers. *daf-16(RNAi)* and the empty vector were
453 used as controls. Proper dauer formation was assessed by observation in a dissecting microscope and by
454 1% SDS resistance. RNAi clones that caused abnormal dauer phenotypes were validated in *daf-2(e1370)*
455 worms. Identity of the dsRNA was confirmed by sequencing (Macrogen, Korea).
456
457 ***daf-9* suppression assays**
458 For preparation of *daf-9*(RNAi) plates, bacterial cultures were grown overnight in LB with 10 µg/ml
459 tetracycline and 50 µg/ml carbenicillin and induced with 4 mM IPTG for 4 h. Cultures were spun down,
460 suspended in 1/10 volume and 30 µl of bacteria were seeded on 3 cm NGM plates made with 1 mM IPTG

461 and 50 µg/ml carbenicillin. Plates were grown overnight at 25°C and stored at 4°C for no more than 2
462 weeks prior to use.
463 L4 stage animals were placed on 3 cm RNAi plates. Two worms per plate were used for *daf-*
464 *7(e1372)*, while three worms were used for *daf-7;chd-7(gk290)* and *daf-7;chd-7(tm6139)*. After 72 h, the
465 adults were removed and plates were replaced at 25°C for 2-3 days. The total number of dauers, L4s,
466 and adults were then assessed.
467
468 **SDS survival assay**
469 Young adults were transferred to seeded plates and permitted to lay eggs for 5 days at 25°C. The
470 arrested progeny were then washed off plates with M9 (22 mM KH_2PO_4, 42 mM Na_2HPO_4, 85.5 mM
471 NaCl, 1 mM $MgSO_4$) into 15 ml glass conical tubes. Collected animals were washed 2-3 times with M9
472 and the excess liquid was aspirated off. Animals were then treated with 2 ml of 1% SDS for 30 min on a
473 nutator at 25ºC. Following incubation, the samples were washed 3 times with M9 and any excess liquid
474 was aspirated off. Animals were aliquoted to 5 seeded plates with 50-70 worms per plate and allowed to
475 recover at 16°C. The recovered animals were then quantified, and the percentage recovered was
476 calculated. This was repeated 3 times for each strain tested. Comparisons were performed using the χ-
477 squared Test in R; P values were corrected using the Bonferroni method for multiple comparisons.
478
479 ***fog-2* mating assay**
480 To determine if males were capable of siring offspring, 8 males from each strain tested were
481 plated with 4 *fog-2(q71)* adult females on seeded 10 cm plates**.** After 24 h, *fog-2* females were transferred
482 to new plates and within 48 h the proportion of fertile females were scored. Assay was repeated two
483 times.
484
485 **Lifespan assays**
486 All lifespan experiments were conducted by transferring 1 day-old adults from 15°C to 20°C for
487 the remainder of the lifespan assay. NGM plates were seeded with *E. coli* OP50-1. ~150 L4
488 hermaphrodites were transferred to 5 plates per experiment. Every 48 h, animals were scored as alive,
489 dead or censored (animals that exploded, died from bagging or dried out at the edges of the plates).
490 Animals were considered dead when they did not respond to a soft touch to the head with a pick. To
491 prevent the progeny from interfering with the assay, adults were transferred to fresh plates every 48 h
492 until egg production ceased. For *glp-1(e2144)* assays, eggs were kept at 20°C for 4 h and then
493 transferred at 25.5°C for 72 h to induce sterility and switched to 20°C for the remainder of the experiment.
494 Lifespan data were analyzed using the Kaplan-Meier method. Statistics were calculated using the Mantel-
495 Cox nonparametric log-rank method using OASIS2 (81).
496

497 **Pathogen resistance assay**

498 The pathogenic bacterial strain used in this study was *Pseudomonas aeruginosa* (strain PA14).
499 This strain was streaked from a frozen stock onto an LB agar plate, incubated at 37°C overnight and then
500 kept at 4°C (shelf-life of one week). For survival assay, a single PA14 colony was inoculated in King's
501 broth and incubated at 37°C overnight with shaking. 20 µl of this culture was seeded onto slow killing
502 NGM plates (containing 0.35% peptone instead of 0.25%) and incubated for 24 h at 37°C. The plates
503 were then left to sit at room temperature for 24 h. The following day, 150 L4 hermaphrodites grown at
504 15°C were distributed onto five PA14 plates and incubated at 25°C. Survival was monitored at intervals of
505 6-12 h and live, dead and censored animals were recorded. Data and statistics were analyzed using the
506 Kaplan-Meier method as described in the section "Lifespan assays".

507

508 **Microscopy and fluorescence imaging**

509 For imaging dauers and adults, worms were immobilized in a 25 mM sodium azide solution on
510 fresh 4% agarose pads and imaged at 10x and 20x magnification. Images were collected using a Zeiss
511 Axioplan Imaging Microscope with a DIC system and Zeiss Plan-Neofluar 10x and 20x objectives lens.
512 Images were acquired with a Micropublisher 3.3 camera (Q Imaging). ImageJ (NIH) software was used to
513 quantify worm size.

514 For imaging *pCHD-7::mCherry* fluorescence, worms were immobilized with 1 mM levamisole on
515 fresh 2% agarose pads and imaged immediately using a Nikon A1r confocal microscope equipped with a
516 40x PLAN APO oil objective. ImageJ (NIH) software was used to quantify fluorescence intensity.

517 For imaging gonads in *daf-2(e1370)* and mutants, young adults were transferred to seeded plates
518 and permitted to lay eggs for 5 days at 25°C to form dauers, then collected and fixed with Carnoy's
519 solution (75 µl EtOH, 37.5 µl Acetate, 12.5 µl Chloroform) and stained with 5 mg/ml DAPI (4′,6-diamidino-
520 2-phenylindole) in PBS. Animals were imaged as 0.5 µm Z-stacks with the Nikon A1r Confocal
521 Microscope with 40x and 60x plan APO oil objectives.

522 For imaging *ajm-1::GFP*, young adults were transferred to seeded plates and allowed to lay eggs
523 for 5 days at 25°C to form dauers. The arrested progeny was then washed off plates with M9 into 15 ml
524 glass conical tubes. Collected animals were washed 2-3 times with M9 and the excess liquid was
525 aspirated off. Animals were then immobilized with levamisole and the seam cells were imaged as Z-
526 stacks by confocal microscopy as described immediately above.

527 For scanning electron microscopy, worms were fixed by immersing in 2.5% glutaraldehyde in
528 PBS for several hours. Worms were washed 3X in PBS then post fixed in aqueous OsO_4 for 1h, then
529 washed 3x in PBS, dehydrated through a graded series of ethanols (30-100%) then chemically dried with
530 2x 10 min incubations in hexamethyldisilazane. Dried worms were sprinkled onto copper double stick
531 tape on aluminum stubs, sputter coated with 3.5 nm gold-palladium alloy then evaluated on a JEOL JEM
532 6335F microscope at 5 kV.

533

534 **Library preparation and RNA-seq**

535 *daf-2(e1370)* and *chd-7(gk290);daf-2(e1370)*, synchronized eggs were kept at 25°C for 10 days
536 and resulting dauers were collected and frozen. Total RNA was extracted with TRIzol (Invitrogen)
537 following the kit´s protocol. cDNA library was prepared with NEBNext Ultra II RNA library prep kit for
538 Illumina (New England Biolabs), and the sequencing carried out using Illumina's HiSeq-2500 sequencer
539 with single-end mode and read length of 50 bp. Five replicates for *daf-2(e1370)* vs. *chd-7(gk290);daf-*
540 *2(e1370)* were sequenced. For data assessment, a quality control with FastQC software (version 0.11.5)
541 was used. First the raw reads that aligned against the *E. coli* genome (K12 genome) were removed. The
542 remaining sequences were aligned against the reference genome of *C. elegans* WS260 using STAR
543 (version 2.5.4a). The number of mapped reads to genes was counted using Htseq (version 0.9.1). Finally,
544 the DEGs were determined using DESeq2 (version 1.20.0) with a cutoff of 0.05 on False Discovery Rate
545 (FDR). R version 3.5.0 (2018-04-23) and Bioconductor version 3.7 with BiocInstaller version 1.30.0 were
546 used. Heatmaps were generated using pheatmap package (version 1.0.12) with hierarchical clustering
547 on the rows with the default options.

548

549 **Genomic Sequencing of *scd-3***

550 A 6 cm plate replete with *scd-3* gravid animals was washed with 1 ml M9 and collected in a glass
551 conical tube. Worms were washed extensively and then placed on a nutator for 1 h to allow remaining gut
552 bacteria to be passed into the medium. Worms were again washed 3-4 times and settled by gravity. The
553 worm pellet was transferred to 1.5 ml tubes and genomic DNA was prepared according to the
554 manufacturer's protocol with the Purelink Genomic DNA Kit (Invitrogen) except that after addition of
555 digestion buffer, worms were pulverized with a microfuge hand dounce prior to incubation at 55°C.
556 Sequencing was performed by Psomagen, Qiagen CLC Genomics Workbench was used to align the
557 DNA against WBcel235 and view the variant.

558

559 **Oil-Red-O (ORO) staining**

560 Dauers grown at 25°C for 5 days were stained for lipids using ORO, as previously described (82).
561 Animals were mounted on a 4% agarose pad and observed in a Zeiss Axioplan brightfield microscope
562 equipped with a Micropublisher 3.3 camera (Q Imaging). Image J (NIH) was used to quantify the amount
563 of lipids in each animal. At least 20 animals of each strain were quantified. Statistical differences was
564 determined by Student's t-test.

565

566 **L1 survival**

567 Experiments were done at 20°C. Eggs were obtained by bleaching of gravid adults and kept
568 under gentle shaking in 5ml sterile M9 supplemented with 0.1µg/ml streptomycin to hatch (16h). To

569 normalize population density, resulting L1 larvae were diluted to obtain 1 larva/µl in 5ml of M9 and kept
570 under constant agitation for the remainder of the experiment. Every 48h, a 100µl aliquot of L1 larvae were
571 spotted onto a NGM plate and then incubated for 72h. Animals were scored as alive if developed beyond
572 the L2 stage. Percentage of the population alive was normalized to day 1 seeded L1 larvae.
573
574 **Gonad staining**
575 Late L4/Young Adult animals from the relevant strains were collected and fixed with Carnoy's
576 solution (75 µl EtOH, 37.5 µl Acetate, 12.5 µl Chloroform) and stained with 5 mg/ml DAPI (4′,6-diamidino-
577 2-phenylindole) in PBS. Animals were imaged as 0.5 µm Z-stacks with the Nikon A1r Confocal
578 Microscope with 20x objective.
579
580 **ChIP-seq analysis**
581 Data from CHD-7 and DAF-16 ChIP-seq generated by ModEncode project was analyzed.
582 Reference for CHD-7-eGFP: https://www.encodeproject.org/experiments/ENCSR010MNU/. Reference for
583 DAF-16-eGFP: https://www.encodeproject.org/experiments/ENCSR946AUI/. Peaks were downloaded in
584 ce10 and annotated using Homer software. Gene lists from the peak calling were generated and used to
585 compare CHD-7 and DAF-16.
586
587 ***Xenopus laevis* embryo manipulation and microinjections**
588 *Xenopus* embryos were obtained by natural mating. Adult frogs' reproductive behavior was
589 induced by injection of human chorionic gonadotropin hormone. Eggs were collected, de-jellied in 3%
590 cysteine (pH 8.0), maintained in 0.1 X Marc's Modified Ringer's (MMR) solution and staged according to
591 Nieuwkoop and Faber (83). The embryos were placed in 3% ficoll prepared in 1 X MMR for
592 microinjection. Chd7 morpholino (*chd7*-MO: 5′-AACTCATCATGCCAGGGTCTGCCAT-3′) specificity has
593 been previously characterized (36). *Chd7*-MO and Standard Control morpholino (St-MO) were provided
594 by Gene Tools, LLC. The cDNA of *X. laevis col2a1* was amplified by PCR from pCMV-Sport 6-*col2a1*
595 (Dharmacon) with primers M13F and M13R. The PCR fragment was digested with *EcoR*V and *Not*I and
596 cloned into pCS2+ previously digested with *Stu*I and *Not*I. Capped mRNAs for *col2a1* were transcribed *in*
597 *vitro* with SP6 using the mMessage mMachine kit (Ambion) following linearization with *Not*I. *Chd7*-MO
598 and *col2a1* mRNA were injected into both D1 blastomeres of 8-cell staged embryos (82) for lethality and
599 morphometrics analysis. *Chd7*-MO was injected into one D1 blastomeres of 8-cell staged embryos for
600 analysis of *col2a1* expression.
601 Whole-mount *in situ* hybridization was carried out as previously described (85). pCMV-Sport 6-
602 *col2a1* (Dharmacon) construct was linearized with *Sal*I and transcribed with T7 for antisense probe
603 synthesis. Morphometrics analyses were done on fixed tadpoles using ImageJ (NIH) software.
604 Morphometric measurements were normalized to the mean of the uninjected group in order to compare

605 between independent experiments. For cartilage staining, stage 45 tadpoles were fixed with MEMFA for
606 24 hours at 4°C, dehydrated into 100% ethanol and stained in 0.01% Alcian blue 8GX in 70%
607 ethanol/30% glacial acetic acid for three nights. Distaining was done in 100% ethanol followed by
608 rehydration in 2% KOH. Animals were cleared in graded glycerol in 2% KOH and skulls were dissected
609 under stereoscope. Images of whole embryos and skulls were collected with a Leica DFC420 camera
610 attached to a Leica L2 stereoscope.
611
612 **RNA preparation and RT-qPCR**
613 For *Xenopus* RNA extraction, 2-cell staged embryos were injected into both blastomeres with 5
614 ng or 10 ng of *chd7*-MO, collected at stage 23 and snap-frozen for later processing. Six embryos were
615 combined for each treatment. For worm RNA extraction, dauers and partial dauers were developed for a
616 week at 25°C. For all the samples, RNA was isolated using RNAzol (Molecular Research). RNA
617 concentration of each sample was measured using a Nanodrop spectrophotometer and 250 ng of RNA
618 was reverse transcribed using qScript cDNA SuperMix (QuantaBio). Quantitative PCR (qPCR) was
619 preformed using the Forget-Me-Not qPCR Master Mix (Biotium) with a BioRad iCycler thermocycler.
620 Amplification was performed using oligonucleotides designed with PerlPrimer software for *col2a1*
621 (Forward 5´ TCCCTGTTGATGTTGAAGCC 3´; Reverse 5´CAATAGTCACCGCTCTTCCA 3´ and ODC
622 primers have been previously described (86) (Forward 5´CAAAGCTTGTTCTACGCATAGCA 3´; Reverse
623 5´GGTGGCACCAAATTTCACACT 3´). The relative expression of *col2a1* was normalized
624 to *ODC* expression and determined via the method previously described (87). *daf-9* was amplified with
625 specific oligos (Forward 5´ATTCCCCACAAAACAATCGAAGAAT 3´; Reverse 5´
626 GAGATTCAAACACGTTTGGATCG 3´) and expression was normalized to the housekeeping gene *cdc-42*
627 (Forward 5´CTGCTGGACAGGAAGATTACG 3´; Reverse 5´ CTGGGACATTCTCGAATGAAG 3´).
628
629 **Ethics Statement**
630 *Xenopus laevis* experiments were carried out in strict accordance with the recommendations in
631 the Guide for the Care and Use of Laboratory Animals of the NIH and also the ARRIVE guidelines. The
632 animal care protocol was approved by the Comisión Institucional para el Cuidado y Uso de Animales de
633 Laboratorio (CICUAL) of the School of Applied and Natural Sciences, University of Buenos Aires,
634 Argentina (Protocol #64).
635
636 **ACKNOWLEDGMENTS**
637 The authors would like to thank Bruno Moretti, Hernan Grecco, Mario Rossi, and Julie Kocherzat
638 for experimental support. DMJ and ASC were supported by the Consejo Nacional de Investigaciones
639 Científicas y Técnicas (CONICET) Doctoral Fellowship Program. DH laboratory was supported by the
640 Agencia Nacional de Promoción Científica y Tecnológica of Argentina (PICT-2016-0269) and CONICET

641 (PIP 1122015 0100731 CO). MCC laboratory was supported by the Agencia Nacional de Promoción
642 Científica y Tecnológica of Argentina (PICT-2013-0381). Funding for this work was also provided by
643 grants from the CHARGE Syndrome Foundation (JLY and DH), The Company of Biologists (DMJ),
644 NIGMS (R01GM104007 to JLY), and NIA (R01AG051659 to AG). This work was supported in part by the
645 Intramural Research Program of the NIH and the National Institute of Diabetes and Digestive and Kidney
646 Diseases (SY).
647
648 **REFERENCES**
649
650 1. L. E. L. M. Vissers, *et al.*, Mutations in a new member of the chromodomain gene family cause
651 CHARGE syndrome. *Nature genetics* **36**, 955–7 (2004).
652 2. R. Balasubramanian, *et al.*, Functionally compromised CHD7 alleles in patients with isolated
653 GnRH deficiency. *Proc Natl Acad Sci U S A* **111**, 17953–17958 (2014).
654 3. H.-G. Kim, *et al.*, Mutations in CHD7, encoding a chromatin-remodeling protein, cause idiopathic
655 hypogonadotropic hypogonadism and Kallmann syndrome. *Am. J. Hum. Genet.* **83**, 511–519 (2008).
656 4. R. Bernier, *et al.*, Disruptive CHD8 Mutations Define a Subtype of Autism Early in Development.
657 *Cell* **158**, 263–276 (2014).
658 5. C. G. A. Marfella, A. N. Imbalzano, The Chd family of chromatin remodelers. *Mutation research*
659 **618**, 30–40 (2007).
660 6. S. A. Patten, *et al.*, Role of Chd7 in Zebrafish: A Model for CHARGE Syndrome. *PLoS One* **7**
661 (2012).
662 7. E. A. Bosman, *et al.*, Multiple mutations in mouse Chd7 provide models for CHARGE syndrome.
663 *Hum Mol Genet* **14**, 3463–3476 (2005).
664 8. C. Tian, *et al.*, Otitis media in a new mouse model for CHARGE syndrome with a deletion in the
665 Chd7 gene. *PloS one* **7**, e34944 (2012).
666 9. G. Daubresse, *et al.*, The Drosophila kismet gene is related to chromatin-remodeling factors and
667 is required for both segmentation and segment identity. *Development* **126**, 1175–1187 (1999).
668 10. D. J. Melicharek, L. C. Ramirez, S. Singh, R. Thompson, D. R. Marenda, Kismet/CHD7 regulates
669 axon morphology, memory and locomotion in a Drosophila model of CHARGE syndrome. *Hum Mol Genet*
670 **19**, 4253–4264 (2010).
671 11. Z. Asad, *et al.*, Rescue of neural crest-derived phenotypes in a zebrafish CHARGE model by
672 Sox10 downregulation. *Hum Mol Genet* **25**, 3539–3554 (2016).
673 12. T. A. McDiarmid, *et al.*, Systematic phenomics analysis of autism-associated genes reveals
674 parallel networks underlying reversible impairments in habituation. *PNAS* **117**, 656–667 (2020).
675 13. W.-R. Wong, *et al.*, Autism-associated missense genetic variants impact locomotion and
676 neurodevelopment in Caenorhabditis elegans. *Hum Mol Genet* **28**, 2271–2281 (2019).

677 14. C. Kenyon, J. Chang, E. Gensch, A. Rudner, R. Tabtiang, A C. elegans mutant that lives twice as
678 long as wild type. *Nature* **366**, 461–464 (1993).
679 15. P. L. Larsen, Aging and resistance to oxidative damage in Caenorhabditis elegans. *Proc Natl*
680 *Acad Sci U S A* **90**, 8905–8909 (1993).
681 16. M. M. Gaglia, C. Kenyon, Stimulation of Movement in a Quiescent, Hibernation-Like Form of
682 Caenorhabditis elegans by Dopamine Signaling. *J Neurosci* **29**, 7302–7314 (2009).
683 17. J. Wang, S. K. Kim, Global analysis of dauer gene expression in Caenorhabditis elegans.
684 *Development* **130**, 1621–1634 (2003).
685 18. E. Cohen, J. Bieschke, R. M. Perciavalle, J. W. Kelly, A. Dillin, Opposing activities protect against
686 age-onset proteotoxicity. *Science* **313**, 1604–1610 (2006).
687 19. A. Meléndez, *et al.*, Autophagy genes are essential for dauer development and life-span
688 extension in C. elegans. *Science* **301**, 1387–1391 (2003).
689 20. R. Christensen, L. de la Torre-Ubieta, A. Bonni, D. A. Colón-Ramos, A conserved PTEN/FOXO
690 pathway regulates neuronal morphology during C. elegans development. *Development* **138**, 5257–5267
691 (2011).
692 21. C. A. Wolkow, K. D. Kimura, M.-S. Lee, G. Ruvkun, Regulation of C. elegans Life-Span by
693 Insulinlike Signaling in the Nervous System. *Science* **290**, 147–150 (2000).
694 22. R. C. Cassada, R. L. Russell, The dauerlarva, a post-embryonic developmental variant of the
695 nematode Caenorhabditis elegans. *Dev Biol* **46**, 326–342 (1975).
696 23. D. L. Riddle, P. S. Albert, "Genetic and Environmental Regulation of Dauer Larva Development"
697 in *C. Elegans II*, 2nd Ed., D. L. Riddle, T. Blumenthal, B. J. Meyer, J. R. Priess, Eds. (Cold Spring Harbor
698 Laboratory Press, 1997) (September 25, 2017).
699 24. P. Ren, *et al.*, Control of C. elegans larval development by neuronal expression of a TGF-beta
700 homolog. *Science* **274**, 1389–1391 (1996).
701 25. D. Park, A. Estevez, D. L. Riddle, Antagonistic Smad transcription factors control the dauer/non-
702 dauer switch in C. elegans. *Development* **137**, 477–485 (2010).
703 26. L. S. da Graca, DAF-5 is a Ski oncoprotein homolog that functions in a neuronal TGF pathway to
704 regulate C. elegans dauer development. *Development* **131**, 435–446 (2003).
705 27. J. H. Thomas, D. A. Birnby, J. J. Vowels, Evidence for parallel processing of sensory information
706 controlling dauer formation in Caenorhabditis elegans. *Genetics* **134**, 1105–1117 (1993).
707 28. W. M. Shaw, S. Luo, J. Landis, J. Ashraf, C. T. Murphy, The C. elegans TGF-β Dauer Pathway
708 Regulates Longevity via Insulin Signaling. *Current Biology* **17**, 1635–1645 (2007).
709 29. T. Liu, K. K. Zimmerman, G. I. Patterson, Regulation of signaling genes by TGFbeta during entry
710 into dauer diapause in C. elegans. *BMC Dev Biol* **4**, 11 (2004).
711 30. S. D. Narasimhan, *et al.*, PDP-1 Links the TGF-β and IIS Pathways to Regulate Longevity,
712 Development, and Metabolism. *PLoS Genet* **7** (2011).

713 31. T. Inoue, J. H. Thomas, Suppressors of transforming growth factor-beta pathway mutants in the
714 Caenorhabditis elegans dauer formation pathway. *Genetics* **156**, 1035–1046 (2000).
715 32. B. Gerisch, A. Antebi, Hormonal signals produced by DAF-9/cytochrome P450 regulate C.
716 elegans dauer diapause in response to environmental cues. *Development* **131**, 1765–1776 (2004).
717 33. H. Y. Mak, G. Ruvkun, Intercellular signaling of reproductive development by the C. elegans DAF-
718 9 cytochrome P450. *Development* **131**, 1777–1786 (2004).
719 34. D. Hochbaum, *et al.*, DAF-12 regulates a connected network of genes to ensure robust
720 developmental decisions. *PLoS Genet* **7**, e1002179 (2011).
721 35. R. A. Ignotz, J. Massagué, Transforming growth factor-beta stimulates the expression of
722 fibronectin and collagen and their incorporation into the extracellular matrix. *J. Biol. Chem.* **261**, 4337–
723 4345 (1986).
724 36. R. Bajpai, *et al.*, CHD7 cooperates with PBAF to control multipotent neural crest formation.
725 *Nature* **463**, 958–962 (2010).
726 37. A. Dubey, J.-P. Saint-Jeannet, Modeling Human Craniofacial Disorders in Xenopus. *Curr*
727 *Pathobiol Rep* **5**, 79–92 (2017).
728 38. D. W. Seufert, J. Hanken, M. W. Klymkowsky, Type II collagen distribution during cranial
729 development in Xenopus laevis. *Anat. Embryol.* **189**, 81–89 (1994).
730 39. P. S. Albert, D. L. Riddle, Mutants of Caenorhabditis elegans that form dauer-like larvae. *Dev Biol*
731 **126**, 270–293 (1988).
732 40. E. S. Haag, Dial-a-mutant: web-based knockout collections for model organisms. *Biol. Cell* **99**,
733 343–347 (2007).
734 41. P. Narbonne, R. Roy, Caenorhabditis elegans dauers need LKB1/AMPK to ration lipid reserves
735 and ensure long-term survival. *Nature* **457**, 210–214 (2009).
736 42. P. Kadekar, R. Roy, AMPK regulates germline stem cell quiescence and integrity through an
737 endogenous small RNA pathway. *PLoS Biol* **17** (2019).
738 43. H. Hsin, C. Kenyon, Signals from the reproductive system regulate the lifespan of C. elegans.
739 *Nature* **399**, 362–366 (1999).
740 44. D. A. Garsin, *et al.*, Long-lived C. elegans daf-2 mutants are resistant to bacterial pathogens.
741 *Science* **300**, 1921 (2003).
742 45. I. Lee, A. Hendrix, J. Kim, J. Yoshimoto, Y.-J. You, Metabolic rate regulates L1 longevity in C.
743 elegans. *PLoS One* **7**, e44720 (2012).
744 46. M. Ailion, J. H. Thomas, Dauer Formation Induced by High Temperatures in Caenorhabditis
745 elegans. *Genetics* **156**, 1047–1067 (2000).
746 47. C. Savage, *et al.*, Caenorhabditis elegans genes sma-2, sma-3, and sma-4 define a conserved
747 family of transforming growth factor beta pathway components. *Proc Natl Acad Sci U S A* **93**, 790–794
748 (1996).

749 48. Y. Suzuki, *et al.*, A BMP homolog acts as a dose-dependent regulator of body size and male tail
750 patterning in Caenorhabditis elegans. *Development* **126**, 241–250 (1999).
751 49. B. Gerisch, C. Weitzel, C. Kober-Eisermann, V. Rottiers, A. Antebi, A hormonal signaling pathway
752 influencing C. elegans metabolism, reproductive development, and life span. *Dev Cell* **1**, 841–851 (2001).
753 50. M. B. Gerstein, *et al.*, Integrative analysis of the Caenorhabditis elegans genome by the
754 modENCODE project. *Science* **330**, 1775–1787 (2010).
755 51. N. A. Noble, J. R. Harper, W. A. Border, In vivo interactions of TGF-beta and extracellular matrix.
756 *Prog Growth Factor Res* **4**, 369–382 (1992).
757 52. U. Madaan, *et al.*, BMP Signaling Determines Body Size via Transcriptional Regulation of
758 Collagen Genes in Caenorhabditis elegans. *Genetics* **210**, 1355–1367 (2018).
759 53. R. P. Boot-Handford, D. S. Tuckwell, Fibrillar collagen: the key to vertebrate evolution? A tale of
760 molecular incest. *Bioessays* **25**, 142–151 (2003).
761 54. W. R. Wilcox, Connective Tissue and Its Heritable Disorders: Molecular, Genetic, and Medical
762 Aspects,. *Am J Hum Genet* **72**, 503–504 (2003).
763 55. A. Wood, D. E. Ashhurst, A. Corbett, P. Thorogood, The transient expression of type II collagen
764 at tissue interfaces during mammalian craniofacial development. *Development* **111**, 955–968 (1991).
765 56. N. Garamszegi, *et al.*, Extracellular matrix-induced transforming growth factor-beta receptor
766 signaling dynamics. *Oncogene* **29**, 2368–2380 (2010).
767 57. W. Xin, J. Heilig, M. Paulsson, F. Zaucke, Collagen II regulates chondroycte integrin expression
768 profile and differentiation. *Connect Tissue Res* **56**, 307–314 (2015).
769 58. L.-H. Chiu, *et al.*, Differential effect of ECM molecules on re-expression of cartilaginous markers
770 in near quiescent human chondrocytes. *J Cell Physiol* **226**, 1981–1988 (2011).
771 59. R. Kerney, B. K. Hall, J. Hanken, Regulatory elements of Xenopus col2a1 drive cartilaginous
772 gene expression in transgenic frogs. *Int J Dev Biol* **54**, 141–150 (2010).
773 60. J. R. Siebert, J. M. Graham, C. MacDonald, Pathologic features of the CHARGE association:
774 Support for involvement of the neural crest. *Teratology* **31**, 331–336 (1985).
775 61. A. Antebi, W. H. Yeh, D. Tait, E. M. Hedgecock, D. L. Riddle, daf-12 encodes a nuclear receptor
776 that regulates the dauer diapause and developmental age in C. elegans. *Genes Dev* **14**, 1512–1527
777 (2000).
778 62. C. L. Hale, A. N. Niederriter, G. E. Green, D. M. Martin, Atypical phenotypes associated with
779 pathogenic CHD7 variants and a proposal for broadening CHARGE syndrome clinical diagnostic criteria.
780 *Am. J. Med. Genet. A* **170**, 344–354 (2016).
781 63. X. Chu, *et al.*, Genotranscriptomic meta-analysis of the CHD family chromatin remodelers in
782 human cancers – initial evidence of an oncogenic role for CHD7. *Mol Oncol* **11**, 1348–1360 (2017).
783 64. M. Murakami, M. Koga, Y. Ohshima, DAF-7/TGF-β expression required for the normal larval
784 development in C. elegans is controlled by a presumed guanylyl cyclase DAF-11. *Mechanisms of*

785 *Development* **109**, 27–35 (2001).
786 65. Y. Liu, *et al.*, CHD7 interacts with BMP R-SMADs to epigenetically regulate cardiogenesis in
787 mice. *Human Molecular Genetics* **23**, 2145–2156 (2014).
788 66. M. Tewari, *et al.*, Systematic Interactome Mapping and Genetic Perturbation Analysis of a C.
789 elegans TGF-NL Signaling Network. *Molecular Cell*, 14.
790 67. C. G. Riedel, *et al.*, DAF-16 employs the chromatin remodeller SWI/SNF to promote stress
791 resistance and longevity. *Nat. Cell Biol.* **15**, 491–501 (2013).
792 68. K. Jia, P. S. Albert, D. L. Riddle, DAF-9, a cytochrome P450 regulating C. elegans larval
793 development and adult longevity. *Development* **129**, 221–231 (2002).
794 69. J. S. Lee, *et al.*, FMRFamide-like peptides expand the behavioral repertoire of a densely
795 connected nervous system. *PNAS* **114**, E10726–E10735 (2017).
796 70. X. Huang, J.-P. Saint-Jeannet, Induction of the neural crest and the opportunities of life on the
797 edge. *Developmental Biology* **275**, 1–11 (2004).
798 71. H. Okuno, *et al.*, CHARGE syndrome modeling using patient-iPSCs reveals defective migration of
799 neural crest cells harboring CHD7 mutations. *Elife* **6** (2017).
800 72. J. M. Kramer, "Extracellular Matrix" in *C. Elegans II*, 2nd Ed., D. L. Riddle, T. Blumenthal, B. J.
801 Meyer, J. R. Priess, Eds. (Cold Spring Harbor Laboratory Press, 1997) (March 22, 2021).
802 73. M. Breuer, M. Rummler, C. Zaouter, B. M. Willie, S. A. Patten, Abnormal craniofacial and spinal
803 bone development with col2a1a depletion in a zebrafish model of CHARGE syndrome. *bioRxiv*,
804 2020.07.10.197533 (2020).
805 74. T. Suzuki, D. Sakai, N. Osumi, H. Wada, Y. Wakamatsu, Sox genes regulate type 2 collagen
806 expression in avian neural crest cells. *Dev Growth Differ* **48**, 477–486 (2006).
807 75. D. He, *et al.*, Chd7 cooperates with Sox10 and regulates the onset of CNS myelination and
808 remyelination. *Nature Neuroscience* **19**, 678–689 (2016).
809 76. A. B. Roberts, B. K. McCune, M. B. Sporn, TGF-β: Regulation of extracellular matrix. *Kidney*
810 *International* **41**, 557–559 (1992).
811 77. A. Tekari, R. Luginbuehl, W. Hofstetter, R. J. Egli, Transforming Growth Factor Beta Signaling Is
812 Essential for the Autonomous Formation of Cartilage-Like Tissue by Expanded Chondrocytes. *PLOS*
813 *ONE* **10**, e0120857 (2015).
814 78. C. Chadjichristos, *et al.*, Down-regulation of human type II collagen gene expression by
815 transforming growth factor-beta 1 (TGF-beta 1) in articular chondrocytes involves SP3/SP1 ratio. *J Biol*
816 *Chem* **277**, 43903–43917 (2002).
817 79. R. S. Kamath, J. Ahringer, Genome-wide RNAi screening in Caenorhabditis elegans. *Methods*
818 **30**, 313–321 (2003).
819 80. L. Timmons, D. L. Court, A. Fire, Ingestion of bacterially expressed dsRNAs can produce specific
820 and potent genetic interference in Caenorhabditis elegans. *Gene* **263**, 103–112 (2001).

821 81. S. K. Han, *et al.*, OASIS 2: Online application for survival analysis 2 with features for the analysis
822 of maximal lifespan and healthspan in aging research. *Oncotarget* **7**, 56147–56152 (2016).
823 82. R. Ratnappan, *et al.*, Germline Signals Deploy NHR-49 to Modulate Fatty-Acid β-Oxidation and
824 Desaturation in Somatic Tissues of C. elegans. *PLoS Genetics* **10** (2014).
825 83. Nieuwkoop, P.D., Faber, J., *Normal Table of Xenopus Laevis (Daudin)* | *Taylor & Francis Group*
826 (Garland Publishing, 1994).
827 84. S. Huang, K. E. Johnson, H. Z. Wang, Blastomeres show differential fate changes in 8-cell
828 Xenopus laevis embryos that are rotated 90 degrees before first cleavage. *Dev Growth Differ* **40**, 189–
829 198 (1998).
830 85. V. Gawantka, *et al.*, Gene expression screening in Xenopus identifies molecular pathways,
831 predicts gene function and provides a global view of embryonic patterning. *Mechanisms of Development*
832 **77**, 95–141 (1998).
833 86. Q. Cao, Y. Shen, W. Zheng, H. Liu, C. Liu, Tcf7l1 promotes transcription of Kruppel-like factor 4
834 during Xenopus embryogenesis. *J Biomed Res* **32**, 215–221 (2018).
835 87. M. W. Pfaffl, A new mathematical model for relative quantification in real-time RT-PCR. *Nucleic*
836 *Acids Res* **29**, e45 (2001).
837

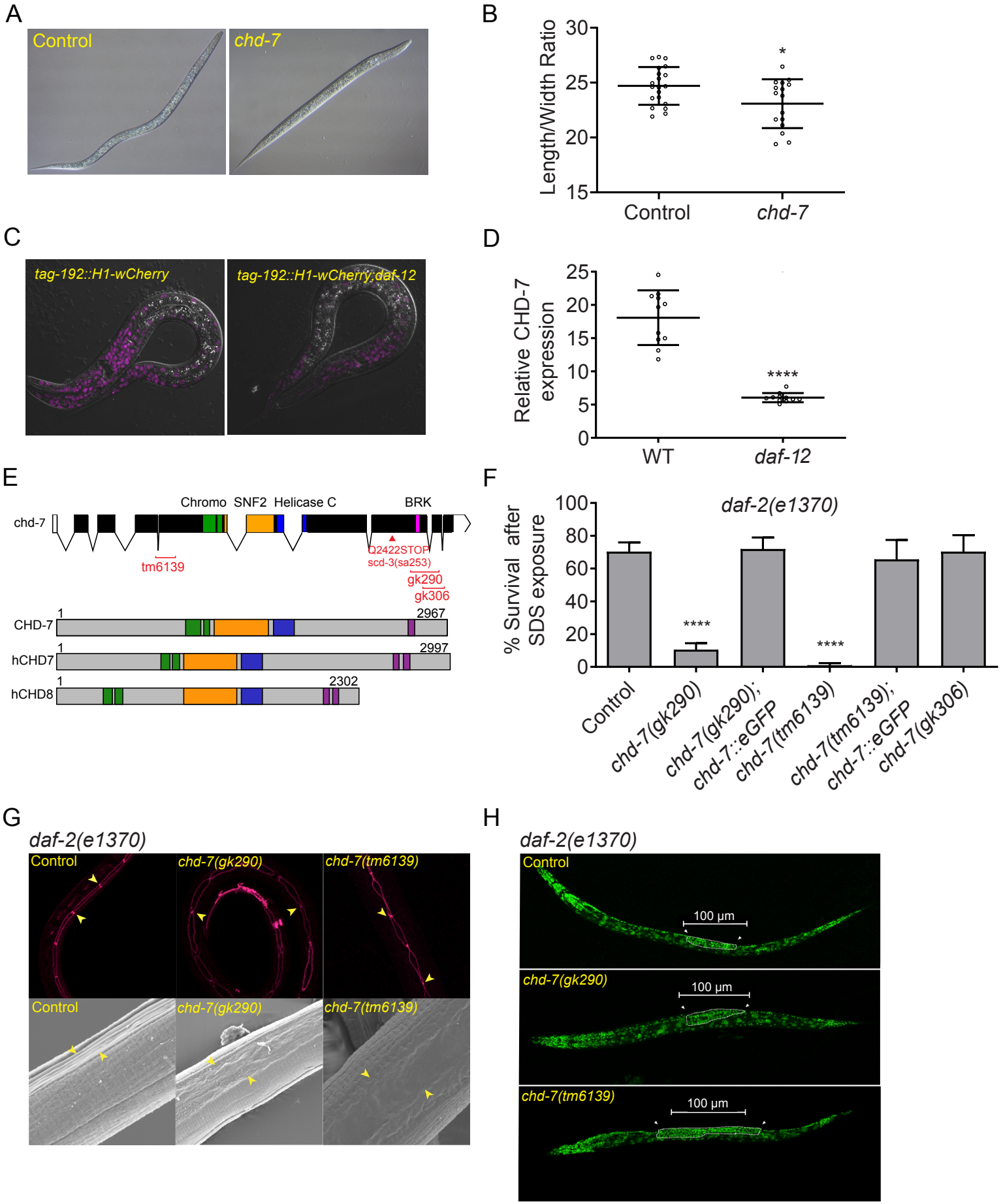

Jofré, DM and Hoffman, D *et al*, Figure 1

838 **Figure 1: The DAF-12 regulated target *chd-7* is required for proper dauer morphogenesis**

839

840 A) *chd-7(RNAi)* causes a partial dauer phenotype in *daf-2(e1370).* Representative DIC photomicrographs
841 of normal and partial dauers from *daf-2(e1370)* exposed to Control (L4440) or *chd-7* dsRNA, respectively.
842 B) Quantification of axial ratio of *daf-2(e1370);*Control(RNAi) and *daf-2(e1370);chd-7(RNAi)* dauers.
843 Three biological replicates were scored (n=16-21/replicate). Horizontal black lines represent mean with
844 SD. Unpaired t test, *p<0.05.
845 C) *daf-12* regulates *chd-7* expression. Representative images of *chd-7* transcriptional reporter, *tag-*
846 *192::H1-wCherry* or *tag-192::H1-wCherry;daf-12(rh61rh411)* worms at L2/L3 stage.
847 D) Relative expression of the translational reporter (n>10/strain). Unpaired t test, ****p<0.0001.
848 E) *C. elegans chd-7* gene and protein. Top: *chd-7* genomic region. UTR and exons shown as bars;
849 introns by lines. In red, available *chd-7* deletional alleles (data obtained from CGC and NBRP). Bottom
850 images depict the predicted protein isoforms of *C. elegans* CHD-7, human CHD7 and human CHD8.
851 Signature domains in CHD proteins: two N-terminal chromodomains for interaction with a variety of
852 chromatin components (green), a SNF-2 like domain with ATPase activity (yellow) and a Helicase domain
853 (blue). The Class III subfamily is defined by a BRK domain (purple).
854 F) *chd-7*(*gk290*);*daf-2(e1370)* and *chd-7*(*tm6139*);*daf-2(e1370)* develop as SDS-sensitive dauer larvae.
855 n>725 animals/strain tested. Bars and horizontal black lines represent mean percentage with SD. Chi-
856 squared test with Bonferroni correction for multiple comparisons. ****p<0.0001. * represents the
857 comparison to the *daf-2(e1370)* strain
858 G) *chd-7* partial dauers fail to develop the dauer alae. Top row, representative photomicrographs of *daf-*
859 *2(e1370)* dauers or *chd-7;daf-2(e1370)* partial dauers expressing the *ajm-1*::GFP reporter to delineate the
860 seam cell borders (arrowheads mark a subset of junctions). Bottom row, SEM images of *daf-2(e1370)*
861 dauers or *chd-7;daf-2(e1370)* partial dauers (arrowheads mark alae details).
862 H) Germ cells in *chd-7;daf-2(e1370)* mutants overproliferate and arrest as L3-like germ cells.
863 Representative Z-projections *daf-2(e1370)* dauers or *chd-7;daf-2(e1370)* partial dauers stained with DAPI
864 (green). Arrowheads denote the anterior and posterior ends of the developing gonad arms.
865

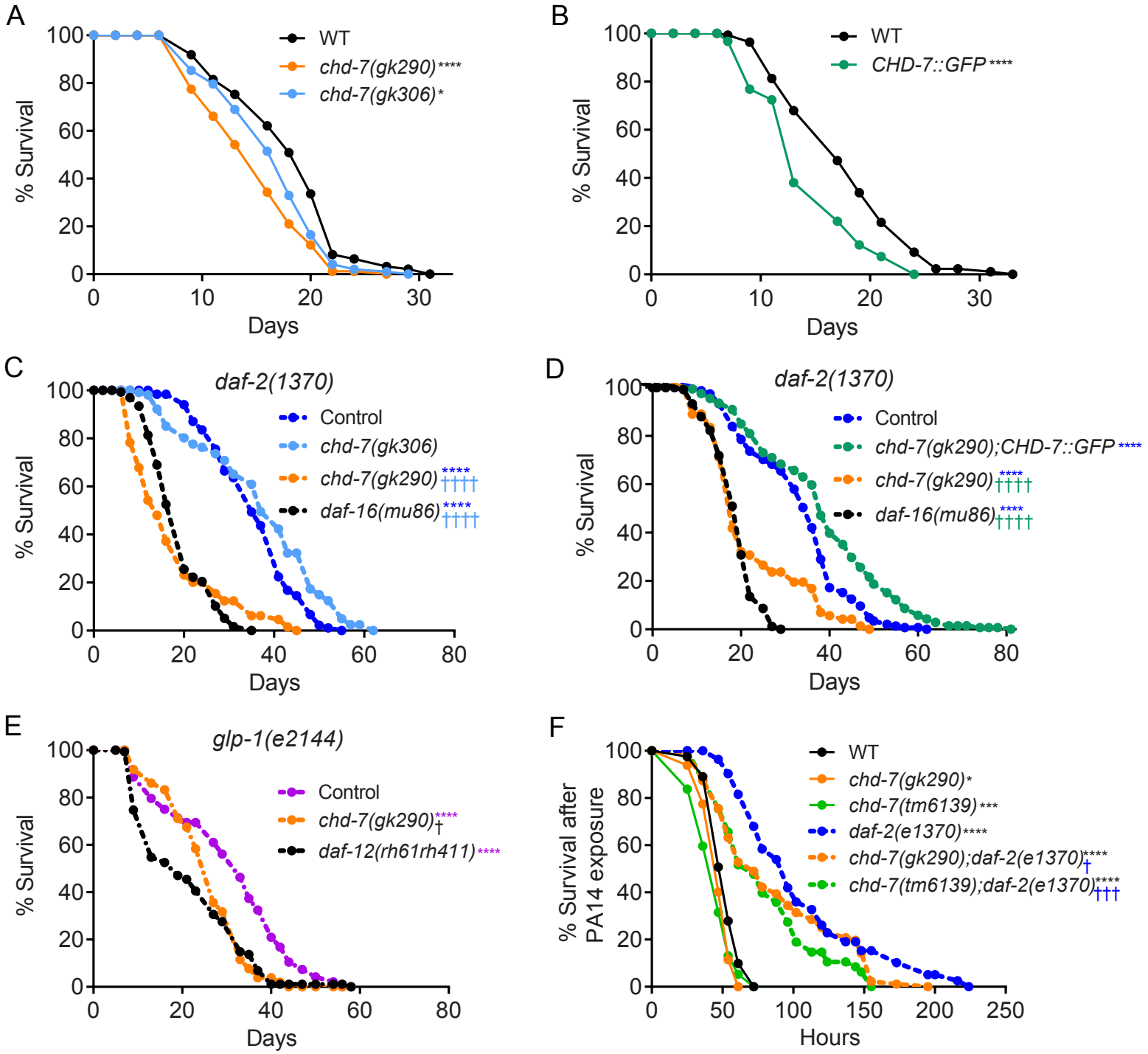

Jofré, DM and Hoffman, D *et al*, Figure 2

866 **Figure 2: *chd-7* affects longevity and response to pathogen.**

867

868 A-E) *chd-7* promotes longevity in wild-type, *daf-2(e1370)* and *glp-1(e2144)* mutants. Mean survival days
869 on OP50-1; survival data analyzed using Kaplan−Meier test.
870 A) WT (18.12 days), *chd-7(gk290*) (14.91), *chd-7(gk306)* (16.53). *p<0.05 and ****p<0.0001 compared to
871 the wild-type, N2 strain.
872 B) WT (17.85), CHD-7::GFP (14.35). ****p<0.0001 compared to the wild-type, N2 strain.
873 C) *daf-2(e1370)* (35.58)*, chd-7(gk306);daf-2(e1370)* (37.18)*, chd-7(gk290);daf-2(e1370)* (17.47)*, daf-*
874 *16(mu86);daf-2(e1370)* (18.85)*.* ****,††††p<0.0001. *represents comparison to *daf-2(e1370)*; †represents
875 comparison to *chd-7(gk306);daf-2(e1370)*.
876 D) *daf-2(e1370)* (27.9)*, chd-7(gk290);daf-2(e1370);CHD-7::GFP* (30.84)*, chd-7(gk290);daf-2(e1370)*
877 (19.13)*, daf-16(mu86);daf-2(e1370)* (14.48)*.* ****,††††p<0.0001. *represents comparison to *daf-2(e1370);*
878 †represents comparison to *chd-7(gk290);daf-2(e1370);CHD-7::GFP*.
879 E) *glp-1(e2144)* (30.4), *chd-7(gk290);glp-1(e2144)* (28.37), *glp-1(e2144);daf-12(rh61rh411)* (25.99). ****p
880 <0.0001 and †p<0.05. *comparison to *glp-1(e2144)*; †comparison to *glp-1(e2144);daf-12(rh61rh411)*.
881 Details of number of animals and other data from replicates found in Supplemental Table 2.
882 F) *chd-7* mediates the response against the opportunistic bacteria *P. aeruginos*a. Mean lifespan in hours
883 (m) ± standard error of the mean (SEM). 'n' is the number of animals analyzed/total number in
884 experiment. WT (m = 52.11 ± 0.96, n = 94/162), *chd-7(gk290)* (m = 47.45 ± 1.05, n = 54.130/), *chd-*
885 *7(tm6139)* (m = 44.47 ± 1.57, n = 56/80), *daf-2(e1370)* (m = 105.46 ± 5.61, n = 65/115), *chd-*
886 *7(gk290);daf-2(e1370)* (m = 86.74 ± 4.21, n = 103/120) and *chd-7(tm6139);daf-2(e1370)* (m = 79.13 ±
887 4.9, n = 50/60). *,†p<0.05; ***,†††p <0.001 and ****p <0.0001. *comparison to N2; †comparison to *daf-*
888 *2(e1370)*. Survival data analyzed using Kaplan−Meier test.
889

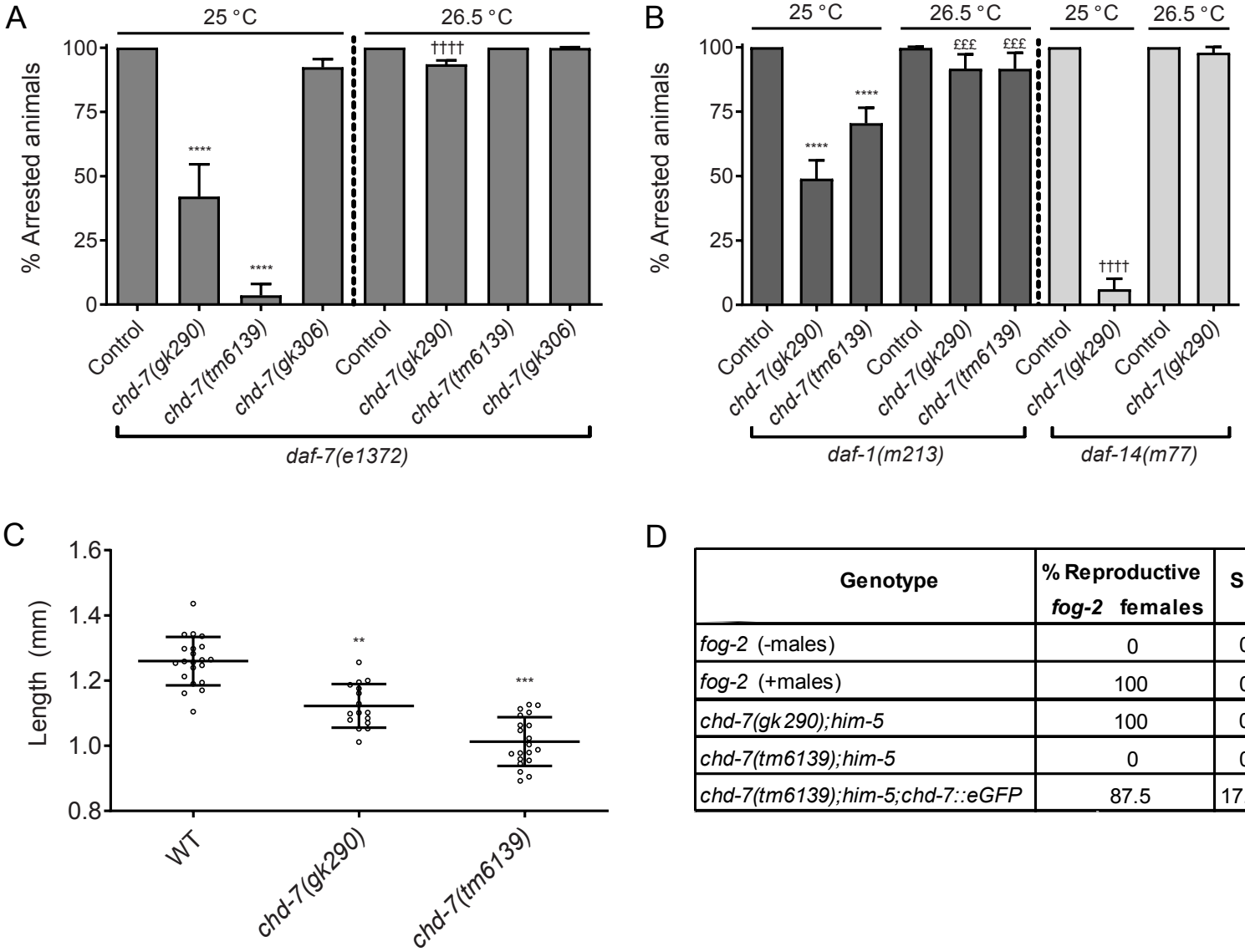

Genotype	% Reproductive *fog-2* females	SD
fog-2 (-males)	0	0
fog-2 (+males)	100	0
chd-7(gk290);him-5	100	0
chd-7(tm6139);him-5	0	0
chd-7(tm6139);him-5;chd-7::eGFP	87.5	17.67

Jofré, DM and Hoffman, D *et al*, Figure 3

890 **Figure 3: CHD-7 belongs to the TGF-β signaling pathway.**

891

892 A-B) Loss of *chd-7* suppresses dauer arrest of TGF-β pathway mutants at 25°C but not 26.5°C. 7 L4's
893 were plated individually and grown at the specified temperature for 1 week when arrested and non-
894 arrested progeny were scored. Bars and horizontal black lines represent mean percentage with SD.
895 Statistical significance was calculated using Chi-squared test with Bonferroni correction for multiple
896 comparisons. ****,††††p<0.0001 and £££ p <0.001.
897 A) Quantification of dauer arrest in *chd-7;daf-7(e1372)* mutants. * comparison to *daf-7(e1372)* grown at
898 25°C and †comparison to *daf-7(e1372)* at 26.5°C.
899 B) Dauer arrest in TGF-β pathway mutant backgrounds. *comparison to *daf-1(m213)* grown at 25°C,
900 †comparison to *daf-14(m77)* at 25°C; $^{£}$comparison to *daf-1(m213)* at 26.5°C.
901 C) *chd-7* regulates body size. Body length of day 1 adults at 20°C (n>16). One-way Anova, **p<0.01,
902 ***p<0.001 compared to wild-type, N2 strain.
903 D) *chd-7(tm6139)* males do not mate. 8 males from each strain tested were plated with 4 *fog-2* females
904 on 10 cm plates. After 24 hrs, *fog-2* females were transferred to new plates and within 48h the proportion
905 of fertile females were scored. Assay was repeated twice.

906

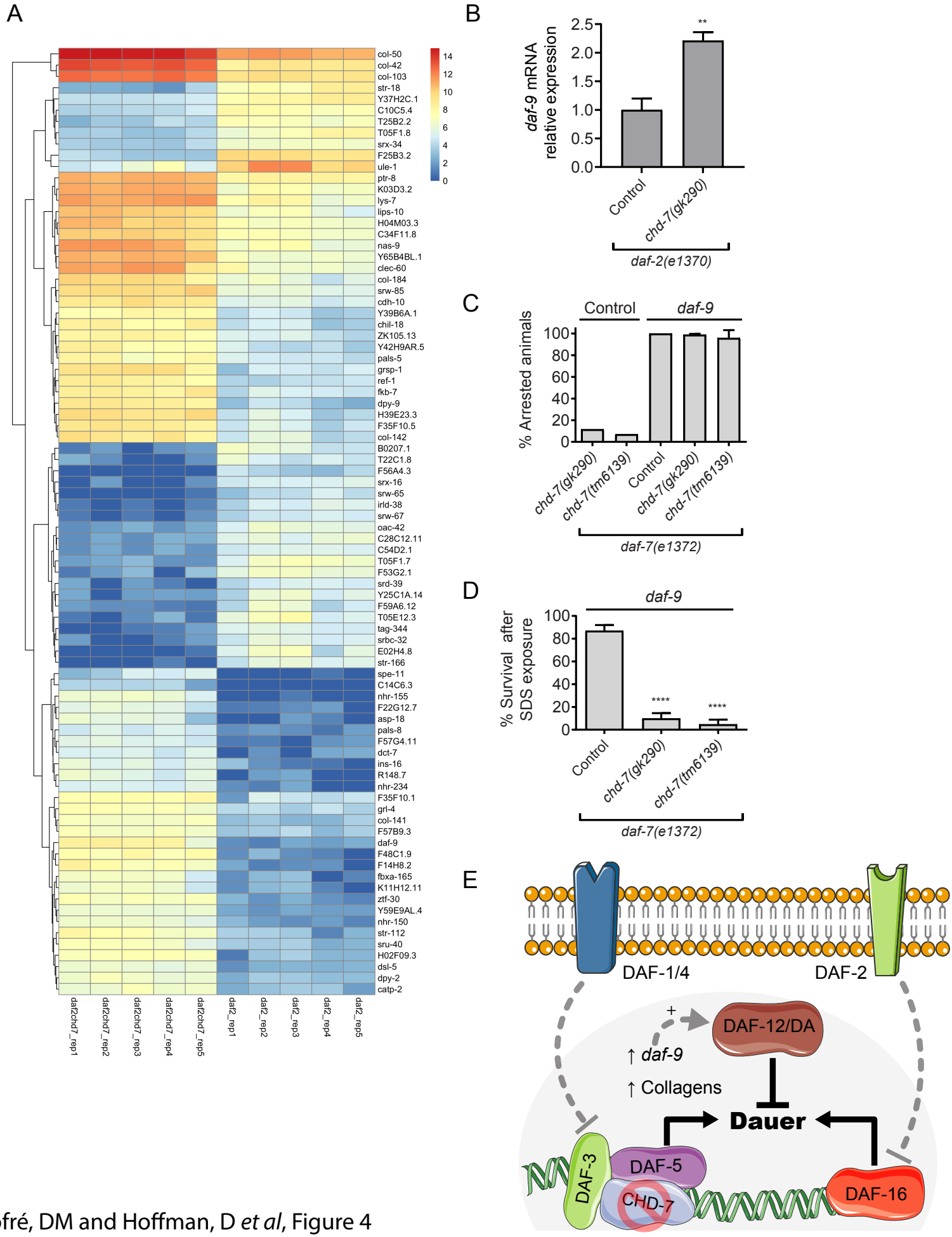

Jofré, DM and Hoffman, D *et al*, Figure 4

907 **Figure 4: RNA-Seq analysis of transcriptome changes in *chd-7(gk290)* mutant dauers.**

908

909 A) Heat map of expression values for the 84 differentially expressed genes (DEGs, cutoff of 0.05 on
910 FDR). DEGs were determined using DESeq2 (version 1.20.0). The color scale represents row z-score.
911 Hierarchical clustering of the DEGs is represented by dendrograms at the left.
912 B) Expression levels of *daf-9* mRNA are increased in *chd-7(gk290);daf-2(e1370)* partial dauers. Error
913 bars indicate standard error from three repeats with different biological samples. Two-tailed unpaired t-
914 test. **p <0.01.
915 C) *daf-9* knockdown in *chd-7*;*daf-7(e1372)* animals rescues dauer arrest at 25°C. 2-3 young L4's were
916 plated on to freshly seeded plates with either *daf-9* or Control empty vector RNAi and allowed to lay eggs.
917 After 72h, the adults were removed and the proportion of progeny that arrested as dauers was calculated.
918 Each dot represents a plate of at least 34 animals (n>598 total animals/ strain). Bars and horizontal black
919 lines represent mean percentage with SD. One-way ANOVA.
920 D) *daf-9* RNAi rescues arrest in *chd-7*;*daf-7(e1372)* animals but leads to partial dauers. Arrested animals
921 grown at 25°C on *daf-9* RNAi plates were treated with 1% SDS for 30 min and survival was scored.
922 n>159 total animals/ strain Each dot represents a plate of at least 30 animals and a minimum of 159 total
923 animals per strain tested. Bars and horizontal black lines represent mean percentage with SD. One-way
924 ANOVA, ****p <0.0001, compared to *daf-7(e1372).*
925 E) Proposed mechanism of action for *chd-7* in dauer development. Under dauer-inducing conditions,
926 CHD-7 forms a transcriptional complex with DAF-3/DAF-5 to repress *daf-9* expression. In *chd-7* mutants,
927 *daf-9* expression prevents dauer formation driven by reduced activity of both DAF-7/TGF-β and DAF-2/IIS
928 signaling pathways, presumably by binding dafachronic acids (DA) and subsequent activation of DAF-12.
929

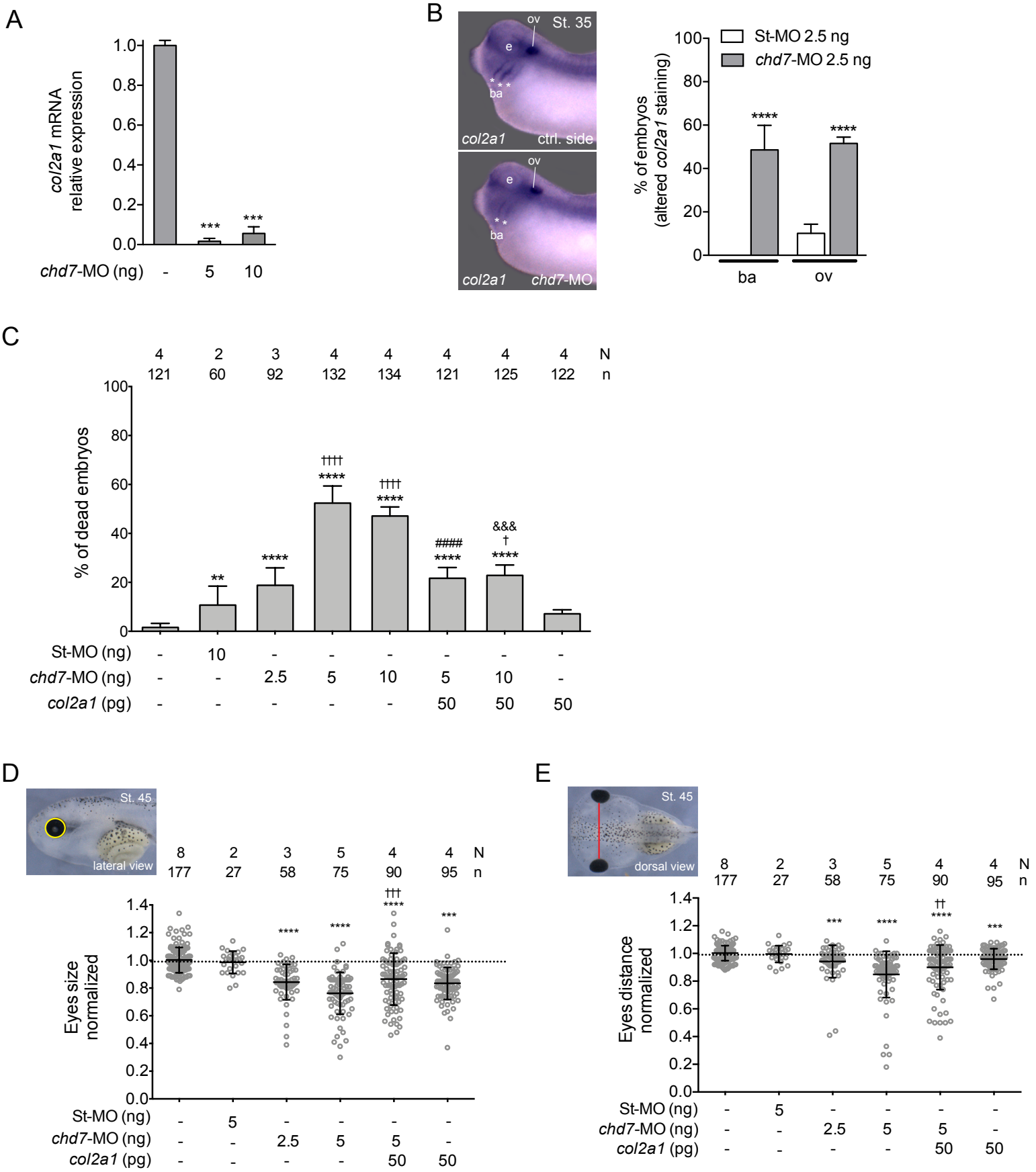

Jofré, DM and Hoffman, D *et al*, Figure 5

930 **Figure 5: Expression of *col2a1* rescues Chd-7 knock-down in *Xenopus* embryos.**

931

932 A) Expression levels of *col2a1* mRNA are reduced in *chd7*-MO injected embryos. Both blastomeres of 2-
933 cell staged embryos were injected with 5 or 10 ng of *chd7*-MO. Error bars indicate standard error from two
934 repeats of the PCR reaction with different biological samples. One-tailed paired t-test, ***$p < 0.001$.
935 B) *Col2a1* expression domain is altered in the branchyal arches (ba) and otic vesicle (ov) of Chd7-
936 depleted embryos. *In situ* hybridization of stage (St.) 35 embryos for *col2a1*. Lateral views, anterior to the
937 left. One D1 blastomeres of 8-cell staged embryos was injected with 2.5 ng of St-MO or *chd7*-MO (N = 2;
938 42 and N = 3; 71, respectively) (N = number of experiments; number of embryos). Top and bottom panels
939 are control and injected sides of the same representative *chd7*-MO injected embryo, respectively. e: eye.
940 The graph is a quantification of the results. Reduced *col2a1* staining was observed in 18% of St-MO and
941 77% of *chd7*-MO injected embryos. Data on graph is presented as means with standard error. Fisher's
942 exact test (****$p < 0.0001$). * represents comparison to St-MO group.
943 C) Lethality in Chd-7-depleted embryos is rescued by over-expression of *col2a1*. Graph showing the
944 percentage of dead embryos. Both D1 blastomeres of 8-cell staged embryos were injected as indicated in
945 the graph and scored for survival at St. 45. Data on graph is presented as means with standard error.
946 Fisher's exact test ($^{\dagger}p < 0.05$, **$p < 0.01$, $^{\&\&\&}p < 0.001$, $^{****,\dagger\dagger\dagger\dagger,\#\#\#\#}$ $p < 0.0001$). * represents comparison to
947 uninjected group, † represents comparison to St-MO group, $^{\#,\&}$ represent comparison to *chd7*-MO 5 ng
948 and 10 ng, respectively.
949 D-E) Craniofacial morphometric analysis of *Xenopus* tadpoles at St. 45. Embryos were injected as
950 indicated in panel C. Each dot represents a single embryo. Means and standard deviation are indicated.
951 One-way ANOVA and Tukey's multiple comparisons test. D) Quantification of the eye size (top left panel).
952 $^{***,\dagger\dagger\dagger}p < 0.001$, ****$p < 0.0001$. E) Quantification of the eye distance (top left panel). $^{\dagger\dagger}p < 0.01$, ***$p < 0.001$,
953 ****$p < 0.0001$. Lateral views, anterior to the left. * represents comparison to uninjected group and †
954 represents comparison to *chd7*-MO 5 ng injected group. N = number of experiments, n = number of
955 embryos.

SUPPLEMENTAL FIGURES

A

B

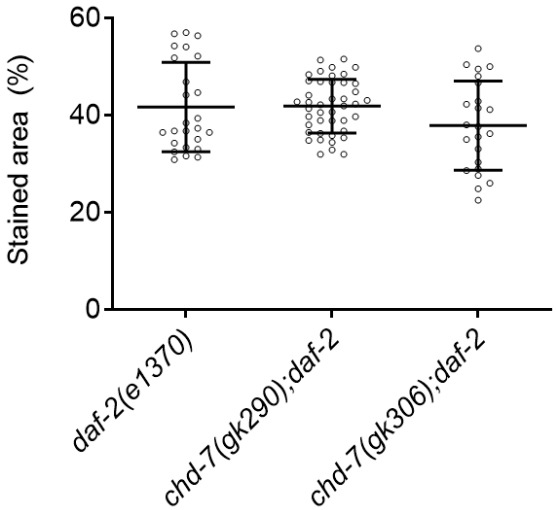

Figure S1: *chd-7* does not affects fat storage. Dauers of the shown genotypes were grown at 25°C for 5 days prior to lipid staining with Oil Red O (ORO). A. Representative photomicrographs of ORO-strained worms. B. Quantification of total area of ORO staining/ worm (Image J, see methods) reveals no significant differences in fat accumulation between control and *chd-7* mutants. Three biological replicates were scored with at least 16 individual dauers per replicate. Horizontal black lines represent mean with SD. P>0.05, Student's t test.

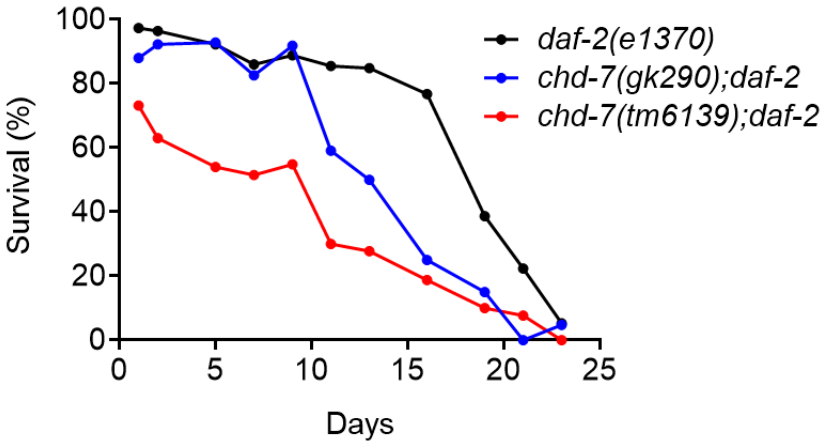

Figure S2: Loss of *chd-7* reduces L1 starvation survival in *daf-2(e1370)* mutants. L1 animals hatched from bleached egg preps into sterile M9 with 0.1µg/ml of streptomycin were diluted to a density of 1 larva/µl and kept at 20°C with constant agitation. Every 48h, 100µl aliquot was spotted onto a seeded NGM plate, and scored 72h later for development beyond the L2 larval stage. Percentage of the population alive was obtained by comparing the initial number of worms at t=0. Each dot represents at least 50 L1 worms.

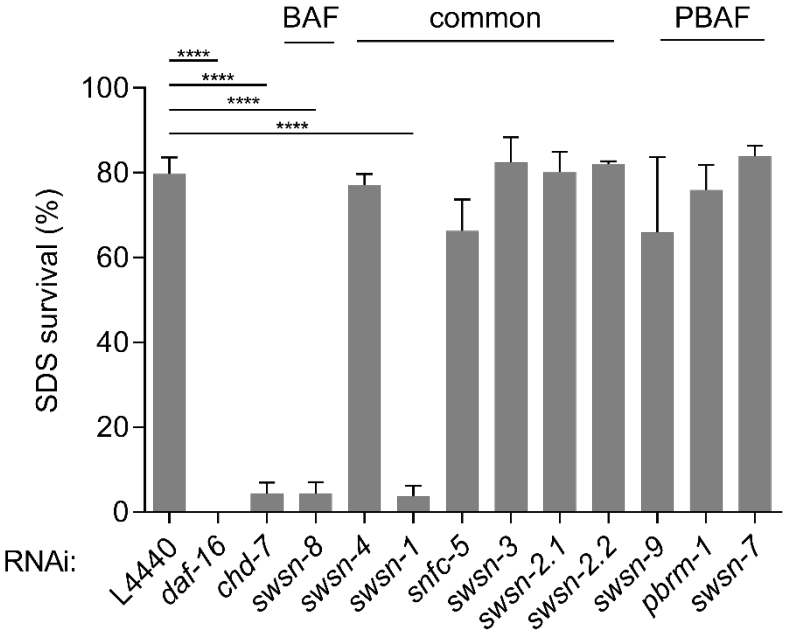

Figure S3*: swsn*-1 *and swsn*-8 share dauer suppression phenotypes with *chd*-7. *daf-7(e1372)* L1 synchronized larvae were placed on the indicated RNAi bacteria and grown at 25°C for 4 days to induce dauer formation. Dauer were identified after 4-5 days based on morphology and their resistance to 1% SDS for 15 min. Common SWI/SNF subunits and BAF or PBAF subclasses are indicated on top. Lines above bars represent standard error of the mean (SEM) from three independent experiments. At least 60 animals were assayed for each RNAi. One-way ANOVA. ****p <0.0001. *comparison to the control, L4440 RNAi.

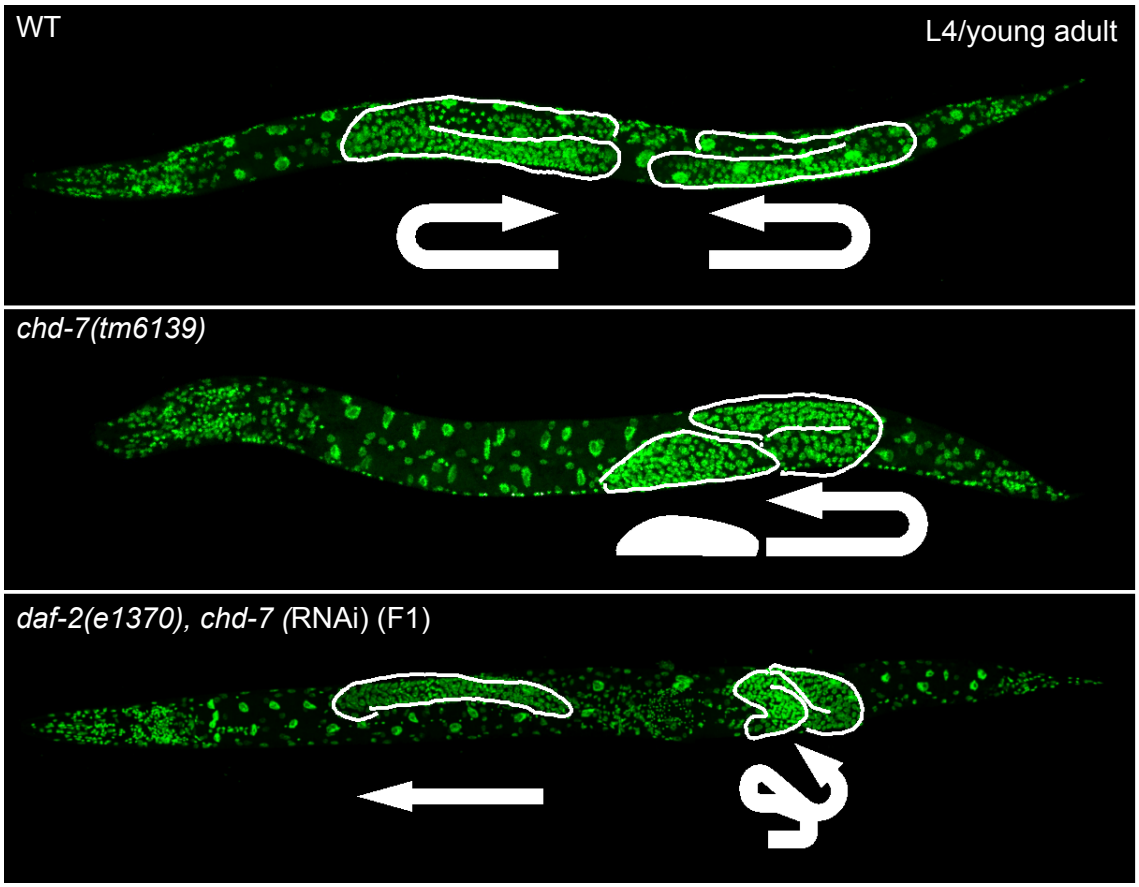

Figure S4: *chd-7* mutants show altered gonad proliferation and migration. Whole mount fixation and DAPI (green) staining of late L4/young adult animals from the relevant strains. RNAi sample was obtained by growing *daf-2(e1370)* for two generations on *chd-7* dsRNA-producing E.Coli.

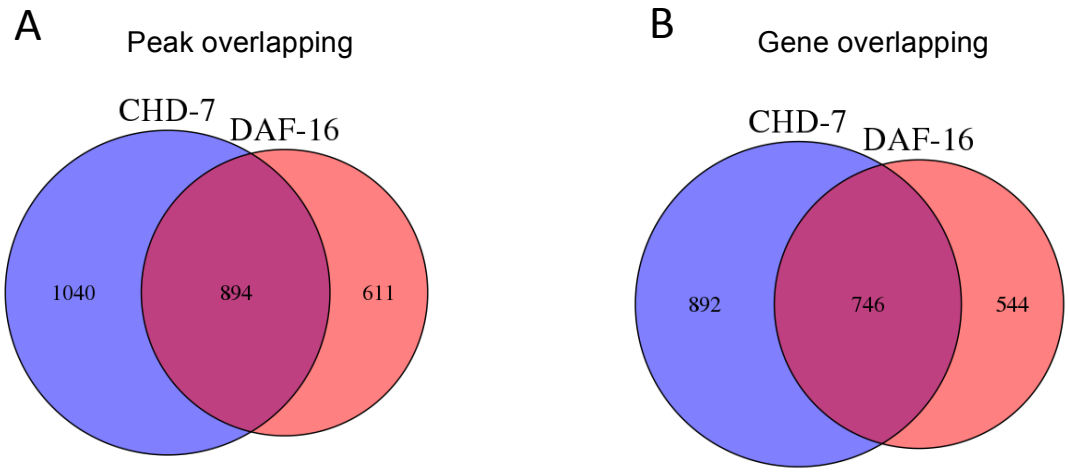

Figure S5: ChIP-seq analysis of CHD-7 and DAF-16 from ModEncode. Comparison of gene lists from peak calling of CHD-7::GFP (young adult) and DAF-16::GFP (L4) using Homer software. A) Venn diagram of ChIP peaks for CHD-7 and DAF-16. Overlap was defined as sharing at least one base in common. B) Common genes shared by CHD-7::GFP and DAF-16::GFP peaks. CHIP-seq data was obtained from publicly available data from the ModEncode project.

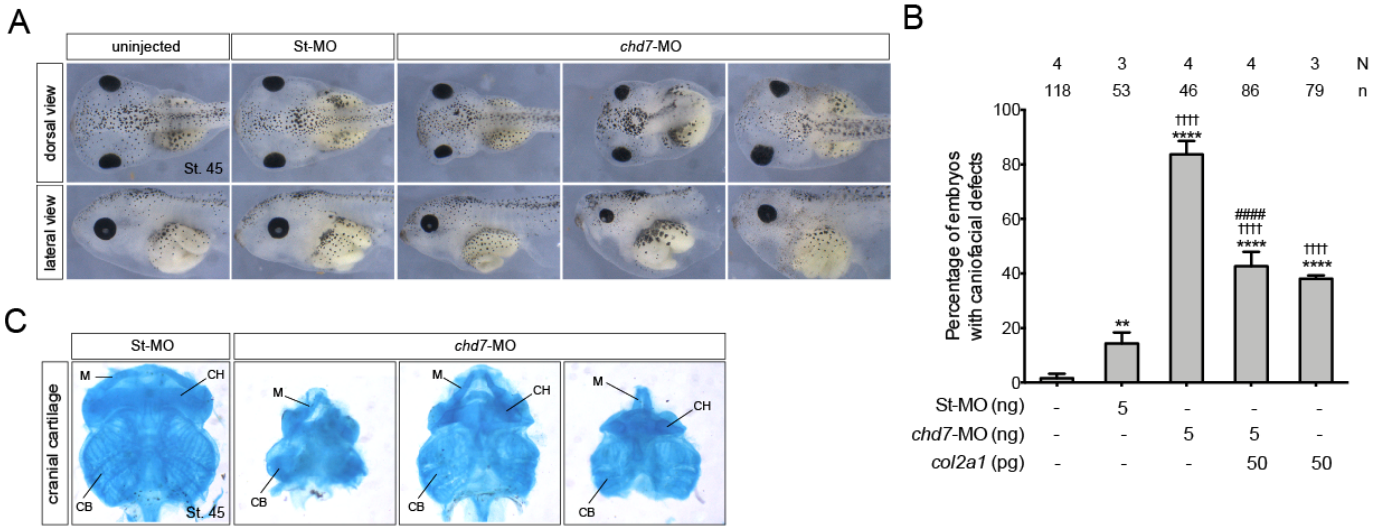

Figure S6: Craniofacial defects of *Chd7* knock-down *Xenopus* tadpoles. A) Gross morphology of surviving tadpoles at St. 45. Embryos were injected into both D1 blastomeres at the 8-cell stage with St-MO (5 ng) and *chd7*-MO (5 ng) as indicated. Tadpoles position is anterior to the left. Embryos are representative. B) Quantification of *Xenopus* tadpoles with craniofacial defects at stage 45. Embryos were injected as indicated in A and in the graph. Data on graph is presented as means with standard error. Fisher's exact test (**p< 0.01, ****,††††,####p< 0.0001). *comparison to uninjected group, † comparison to St-MO group, # comparison to *chd7*-MO group. N = number of experiments, n = number of embryos. C) Examples of Alcian blue-stained craniofacial skeletal elements from St. 45 tadpoles injected with St-MO (5 ng) and *chd7*-MO (5 ng). M: Meckel's, CH: ceratohyle and CB: ceratobranchial cartilages. *chd7*-MO injected tadpoles presented a high incidence of gross head malformations, reduced head and eyes sizes, and abnormal development of craniofacial cartilages.